Langtaosha (LTS) Preprint doi: https://doi.org/10.65215/LTSpreprints.2026.11.27.000404. This version posted November 27, 2026. The copyright holder for this preprint (which was not certified by peer review) is the author/funder. Creative Commons license: CC Attribution-NonCommercial-NoDerivatives 4.0 https://creativecommons.org/licenses/by-nc-nd/4.0

Targeting gut microbial BCAA biosynthesis improves insulin sensitivity in mice

Mingwei Cai[1,9,*], Miaomiao Qin[1,9], Feng Liu[2,9], Jiayong Huang[3], Meihan Liu[1], Yanhao Hu[4], Chunhong Yan[1], Zhen Hui[1,5], Ping Wang[2], Youzhe Chen[1], Xiaolin Zou[1,6], Tianyuan Yu[1], Mengsi Sun[7], Bo He[4], Yonghao Ye[4], Jiahai Zhou[3], and Xiaoyu Tang[1,8,10,*]

Affiliation

[1]Institute of Chemical Biology, Shenzhen Bay Laboratory, Shenzhen 518132, China

[2]Endocrinology and Metabolism Department, Shenzhen University of Advanced Technology General Hospital, Shenzhen 518106, China

[3]State Key Laboratory of Microbial Technology, Nanjing Normal University, Nanjing 210023, China

[4]State Key Laboratory of Agricultural and Forestry Biosecurity, State & Local Joint Engineering Research Center of Green Pesticide Invention and Application, College of Plant Protection, Nanjing Agricultural University, Nanjing 210095, China

[5]Department of Chemistry, School of Science, The Hong Kong University of Science and Technology, Hong Kong 999077, China

[6]Department of Chemistry and The Swire Institute of Marine Science, The University of Hong Kong, Hong Kong 999077, China

[7]Biomedical Research Core Facilities, Shenzhen Bay Laboratory, Shenzhen 518132, China

[8]Shenzhen Medical Academy of Research and Translation, Shenzhen 518107, China

[9]These authors contributed equally

[10]Lead contact

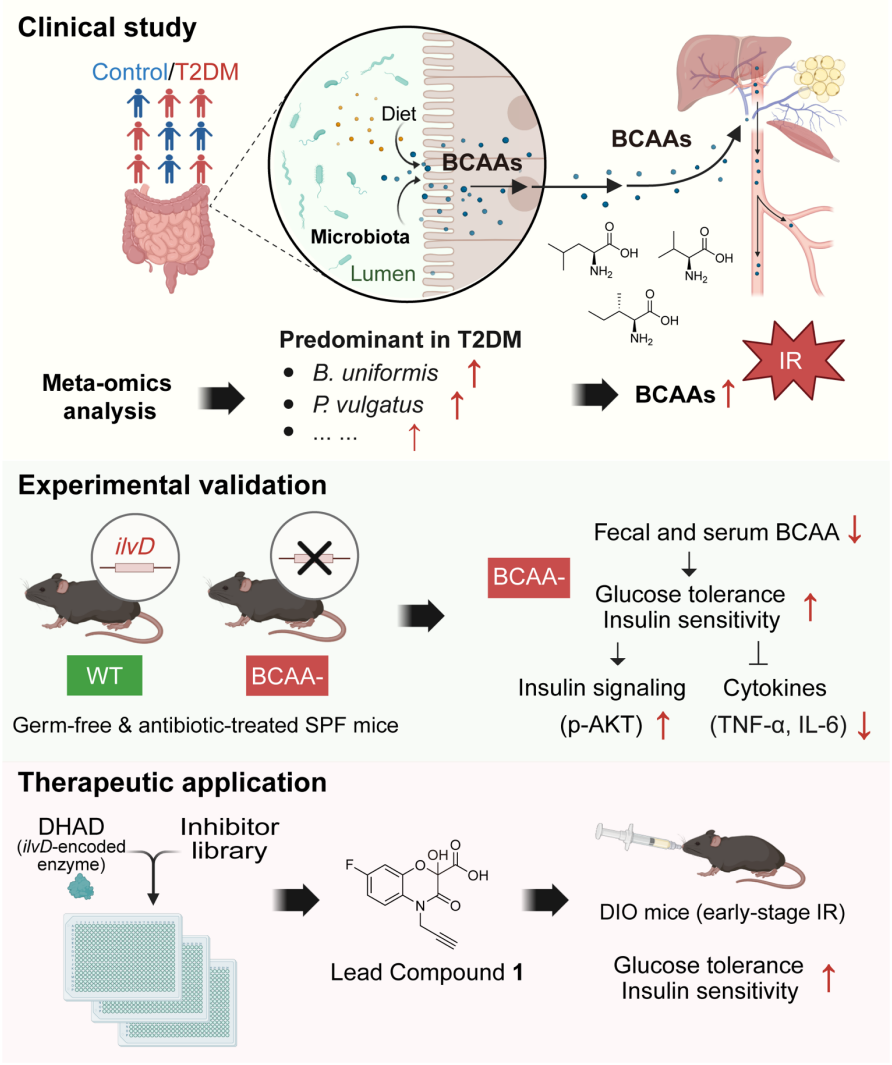
***Correspondence**

xtang@microbechembio.org (X.T.)

ytcaimingwei@gmail.com (M.C.)

Langtaosha (LTS) Preprint doi: https://doi.org/10.65215/LTSpreprints.2026.11.27.000404. This version posted November 27, 2026. The copyright holder for this preprint (which was not certified by peer review) is the author/funder. Creative Commons license: CC Attribution-NonCommercial-NoDerivatives 4.0 https://creativecommons.org/licenses/by-nc-nd/4.0

Graphic Abstract



Highlights

- Multi-omics reveals elevated BCAA biosynthetic capacity in T2DM microbiomes.
- Genetic disruption of microbial BCAA biosynthesis improves insulin sensitivity in mice.
- DHAD is a conserved enzyme across diverse gut bacteria and can be pharmacologically inhibited.
- DHAD inhibition reduces microbial BCAA production and improves insulin sensitivity in mice.

Langtaosha (LTS) Preprint doi: https://doi.org/10.65215/LTSpreprints.2026.11.27.000404. This version posted November 27, 2026. The copyright holder for this preprint (which was not certified by peer review) is the author/funder. Creative Commons license: CC Attribution-NonCommercial-NoDerivatives 4.0 https://creativecommons.org/licenses/by-nc-nd/4.0

In Brief

Cai et al. show that gut microbial branched-chain amino acid (BCAA) biosynthesis contributes to impaired insulin sensitivity in mice. Genetic disruption of BCAA biosynthesis in representative gut bacteria reduces microbial BCAA production and improves host insulin sensitivity. They further identify inhibitors of the conserved BCAA biosynthetic enzyme dihydroxy-acid dehydratase (DHAD) that suppress microbial BCAA production and improve insulin sensitivity in mice. These findings establish the feasibility of pharmacologically targeting microbial BCAA biosynthesis and identify DHAD as a potential target for microbiome-directed intervention.

Langtaosha (LTS) Preprint doi: https://doi.org/10.65215/LTSpreprints.2026.11.27.000404. This version posted November 27, 2026. The copyright holder for this preprint (which was not certified by peer review) is the author/funder. Creative Commons license: CC Attribution-NonCommercial-NoDerivatives 4.0 https://creativecommons.org/licenses/by-nc-nd/4.0

Summary

Insulin resistance underlies type 2 diabetes mellitus (T2DM), yet the contribution of gut microbial metabolism to host insulin sensitivity remains poorly defined. Here, we identify gut microbial branched-chain amino acid (BCAA) biosynthesis as a pathway contributing to impaired insulin sensitivity. Genetic disruption of BCAA biosynthesis in representative gut bacteria reduces microbial BCAA production and improves insulin sensitivity in mice. Comparative genomic and experimental analyses show that BCAA biosynthetic capacity is widely distributed across diverse gut bacteria. Small-molecule inhibition of the conserved BCAA biosynthetic enzyme dihydroxy-acid dehydratase (DHAD) suppresses microbial BCAA production and improves insulin sensitivity in diet-induced obese mice. In individuals with T2DM, fecal BCAA levels and the abundance of representative BCAA-producing bacteria are elevated. Together, these findings establish the feasibility of pharmacologically targeting gut microbial BCAA biosynthesis and identify DHAD as a potential target for microbiome-directed intervention.

Langtaosha (LTS) Preprint doi: https://doi.org/10.65215/LTSpreprints.2026.11.27.000404. This version posted November 27, 2026. The copyright holder for this preprint (which was not certified by peer review) is the author/funder. Creative Commons license: CC Attribution-NonCommercial-NoDerivatives 4.0 https://creativecommons.org/licenses/by-nc-nd/4.0

INTRODUCTION

Insulin resistance (IR), characterized by impaired insulin responsiveness in key metabolic tissues, including the liver, skeletal muscle, and adipose tissue, is a defining feature of type 2 diabetes mellitus (T2DM) and contributes to a broad spectrum of cardiometabolic diseases.[1] Diabetes affects more than 537 million adults worldwide, with its prevalence projected to rise to 783 million by 2045.[2] Current host-directed therapies improve glycemic control, but sustained restoration of insulin sensitivity remains challenging.[3] These limitations highlight the need to identify additional mechanisms that regulate insulin sensitivity and may provide alternative points for therapeutic intervention.

Beyond established genetic and lifestyle determinants, the gut microbiota has emerged as an important regulator of host metabolic homeostasis through its diverse metabolic activities.[4-11] Elevated circulating branched-chain amino acids (BCAAs) are well-known contributors to IR, yet previous studies have primarily focused on dietary BCAA intake,[12,13] host BCAA metabolism,[14] or microbial BCAA utilization.[15,16] Mechanistically, excess BCAAs impair insulin signaling through mTORC1 activation.[9,10,17] Importantly, clinical tracer studies demonstrate that the gut microbiota contributes 19–22% of circulating leucine in adult humans,[18] suggesting that microbial metabolism may substantially influence systemic BCAA homeostasis. However, whether *de novo* BCAA biosynthesis by the gut microbiota contributes to IR remains unclear.[15] Specifically, it is unknown whether gut microbial BCAA biosynthesis contributes to systemic BCAA accumulation, which gut bacteria mediate this process, and whether it causally contributes to impaired host insulin sensitivity.

Given the pathogenic association between elevated circulating BCAAs and IR, targeting BCAA metabolism has emerged as a potential therapeutic strategy.[19] However, recent human genetic studies indicate that modulation of host BCAA catabolism is unlikely to reduce T2DM risk,[20] suggesting that elevated BCAA levels associated with metabolic disease may arise, at least in part, from mechanisms beyond host BCAA metabolism. Targeting microbial metabolic activities has emerged as a promising strategy for modulating host physiology and treating disease.[21-24] Whether microbial BCAA biosynthesis can similarly be targeted to improve metabolic dysfunction remains unknown.

Here, we combine human microbiome analyses, microbial genetics, animal models, comparative genomics, and chemical approaches to investigate the contribution of gut microbial BCAA biosynthesis to IR (Figure 1A). Genetic disruption of the BCAA biosynthetic enzyme dihydroxy-acid dehydratase (DHAD) in representative gut bacteria reduces microbial BCAA production and improves insulin sensitivity in mice. Comparative genomic and experimental analyses further show that BCAA biosynthetic capacity is broadly distributed across phylogenetically diverse gut bacteria and that DHAD is highly conserved

Langtaosha (LTS) Preprint doi: https://doi.org/10.65215/LTSpreprints.2026.11.27.000404. This version posted November 27, 2026. The copyright holder for this preprint (which was not certified by peer review) is the author/funder. Creative Commons license: CC Attribution-NonCommercial-NoDerivatives 4.0 https://creativecommons.org/licenses/by-nc-nd/4.0

among the bacterial orthologs examined. We identify small-molecule DHAD inhibitors that suppress BCAA production across diverse gut bacterial species and improve insulin sensitivity in diet-induced obese mice. Together with human microbiome analyses showing increased BCAA biosynthetic capacity and elevated fecal BCAA levels in individuals with T2DM, these findings establish a functional contribution of gut microbial BCAA biosynthesis to impaired insulin sensitivity in mice and identify DHAD as a potential target for microbiome-directed intervention.

RESULTS

Gut microbial BCAA biosynthetic capacity is enriched in T2DM-associated microbiomes

To systematically identify microbial amino acid biosynthetic pathways associated with T2DM, we performed integrated metagenomic and metatranscriptomic analyses of branched-chain (BCAA), aromatic (AAA), basic (BAA), and sulfur-containing (SCAA) amino acid biosynthetic pathways across 538 human fecal samples (Figure S1 and Table S1). *De novo* assembly yielded 11,867 metagenome-assembled genomes (MAGs), which were dereplicated into 2,894 medium-quality non-redundant representative genomes (Figures 1B, S2A, S2B, and Table S2).

To identify T2DM-associated microbial signatures, we integrated differential abundance analysis with random forest (RF) and support vector machine (SVM) analyses. This approach identified a set of 52 high-confidence T2DM-enriched species clusters, designated Cluster A, that were consistently detected by all three analytical methods (Figure 1C and Table S3). Cluster A was dominated by species belonging to the genera *Bacteroides*, *Phocaeicola*, *Prevotella*, *Enterocloster*, and *Acidaminococcus*, and discriminated individuals with T2DM from controls with an area under the receiver operating characteristic curve (AUC) of 0.70 (95% CI: 0.68–0.71). This microbial signature was further validated across four independent cohorts, with AUC values ranging from 0.60 to 0.82 (Figures S2C and S2D). We therefore focused subsequent analyses on Cluster A.

Langtaosha (LTS) Preprint doi: https://doi.org/10.65215/LTSpreprints.2026.11.27.000404. This version posted November 27, 2026. The copyright holder for this preprint (which was not certified by peer review) is the author/funder. Creative Commons license: CC Attribution-NonCommercial-NoDerivatives 4.0 https://creativecommons.org/licenses/by-nc-nd/4.0

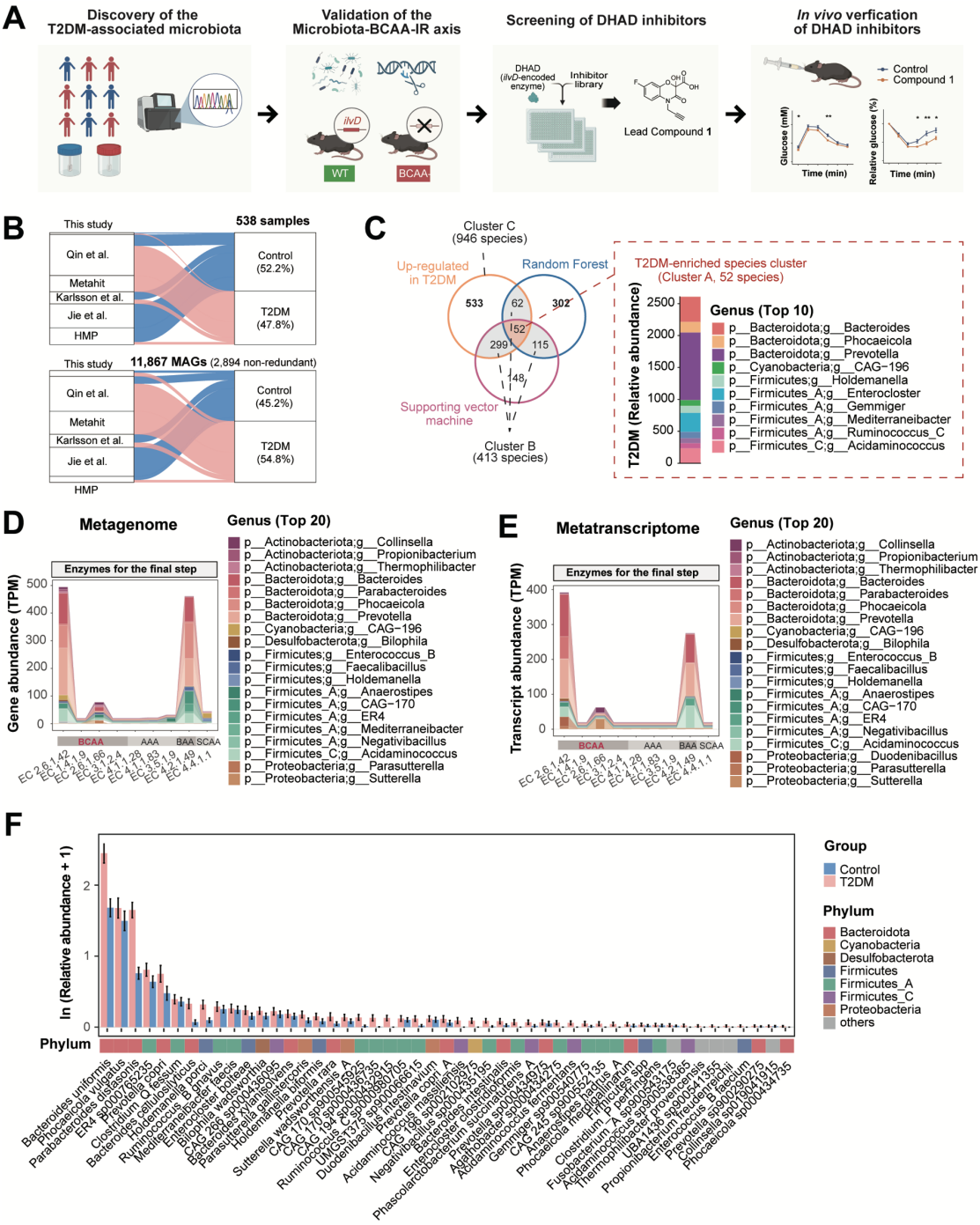


Figure 1. Integrated microbiome multi-omics identifies elevated BCAA biosynthetic capacity in T2DM-associated gut microbiomes.

(A) Schematic overview of the integrated multi-omics discovery, genetic validation, inhibitor development, and therapeutic evaluation workflow.

(B) Overview of study datasets. The upper Sankey diagram shows the distribution of 538 human fecal metagenomic samples from healthy controls and individuals with T2DM across five published cohorts (HMP,[25] Jie et al.,[26] Karlsson et al.,[27] MetaHIT,[28] and Qin et al.[29]) together with the present study. The lower Sankey diagram shows the distribution of the corresponding 11,867 MAGs recovered from these samples according to cohort and disease status.

(C) Venn diagram showing T2DM-associated microbial species clusters identified by differential

Langtaosha (LTS) Preprint doi: https://doi.org/10.65215/LTSpreprints.2026.11.27.000404. This version posted November 27, 2026. The copyright holder for this preprint (which was not certified by peer review) is the author/funder. Creative Commons license: CC Attribution-NonCommercial-NoDerivatives 4.0 https://creativecommons.org/licenses/by-nc-nd/4.0

abundance analysis (edgeR), random forest (RF), and support vector machine (SVM). Cluster A comprises the 52 high-confidence T2DM-enriched species clusters identified by all three analytical approaches and selected for subsequent analyses. Cluster B comprises the 413 T2DM-enriched species clusters that were additionally identified by either RF or SVM. Cluster C comprises the 533 species clusters identified by edgeR as enriched in T2DM. Numeric labels correspond to species clusters detailed in Table S2. The adjacent bar chart shows the genus-level taxonomic composition of Cluster A in T2DM samples, which was quantified using the metaWRAP Quant_bins module and expressed as genome copies per million sequencing reads.

(D and E) Metagenomic (D) and metatranscriptomic (E) profiling of microbial amino acid biosynthetic pathways in Cluster A. Stacked bar plots show the abundance of genes (D) and transcripts (E) encoding enzymes catalyzing the terminal steps of branched-chain (BCAA), aromatic (AAA), basic (BAA), and sulfur-containing (SCAA) amino acid biosynthesis. Colors indicate the genus-level taxonomic assignments of the corresponding genes and transcripts.

(F) Species-level genome abundance of BCAA biosynthesis-associated bacteria in the T2DM and control groups. The relative abundance of each species-level MAG was quantified using the metaWRAP Quant_bins module and expressed as genome copies per million sequencing reads. Abundance values were log-transformed as ln(abundance + 1) for visualization, and data are presented as mean ± SEM. The bottom color strip denotes phylum classification.

Comparative metagenomic and metatranscriptomic profiling of Cluster A showed that BCAA biosynthetic genes and transcripts were consistently more abundant than those associated with the other amino acid biosynthetic pathways examined (Figures 1D, 1E, S2E, and S2F). At the genus level, *Bacteroides*, *Phocaeicola*, *Parabacteroides*, and *Prevotella*—represented by species including *Bacteroides uniformis*, *Phocaeicola vulgatus*, *Parabacteroides distasonis*, *Prevotella copri*, and *Bacteroides xylanisolvens*—collectively accounted for the majority of BCAA biosynthetic genes and transcripts (Figures 1D–1F, S2E–S2G, S3, and Table S4). Together, these findings identify BCAA biosynthesis as a prominent amino acid biosynthetic feature of T2DM-associated gut microbiomes.

Construction of *ilvD*-knockout mutants with reduced BCAA production

Building on the identification of *B. uniformis* and *P. vulgatus* as representative T2DM-enriched bacteria with BCAA biosynthetic capacity, we next genetically tested the contribution of microbial BCAA biosynthesis to host insulin sensitivity. We selected *B. uniformis* DSM 6597 and *P. vulgatus* ATCC 8482 based on their high genomic similarity to the corresponding clinical MAGs (Figure S4). Using a CRISPR-Cas12a-mediated gene editing system, we generated isogenic mutants (*Bu* Δ*ilvD* and *Pv* Δ*ilvD*) by deleting *ilvD*, which encodes dihydroxy-acid dehydratase (DHAD), a key enzyme in BCAA biosynthesis (Figures 2A and 2B). The Δ*ilvD* mutants showed no apparent alterations in cellular morphology (Figure 2C) and only minor changes in growth kinetics (Figure 2D). Consistent

Langtaosha (LTS) Preprint doi: https://doi.org/10.65215/LTSpreprints.2026.11.27.000404. This version posted November 27, 2026. The copyright holder for this preprint (which was not certified by peer review) is the author/funder. Creative Commons license: CC Attribution-NonCommercial-NoDerivatives 4.0 https://creativecommons.org/licenses/by-nc-nd/4.0

with disruption of BCAA biosynthesis, extracellular concentrations of leucine, isoleucine, and valine were markedly reduced in both Δ*ilvD* strains compared with their wild-type counterparts (Figure 2E).

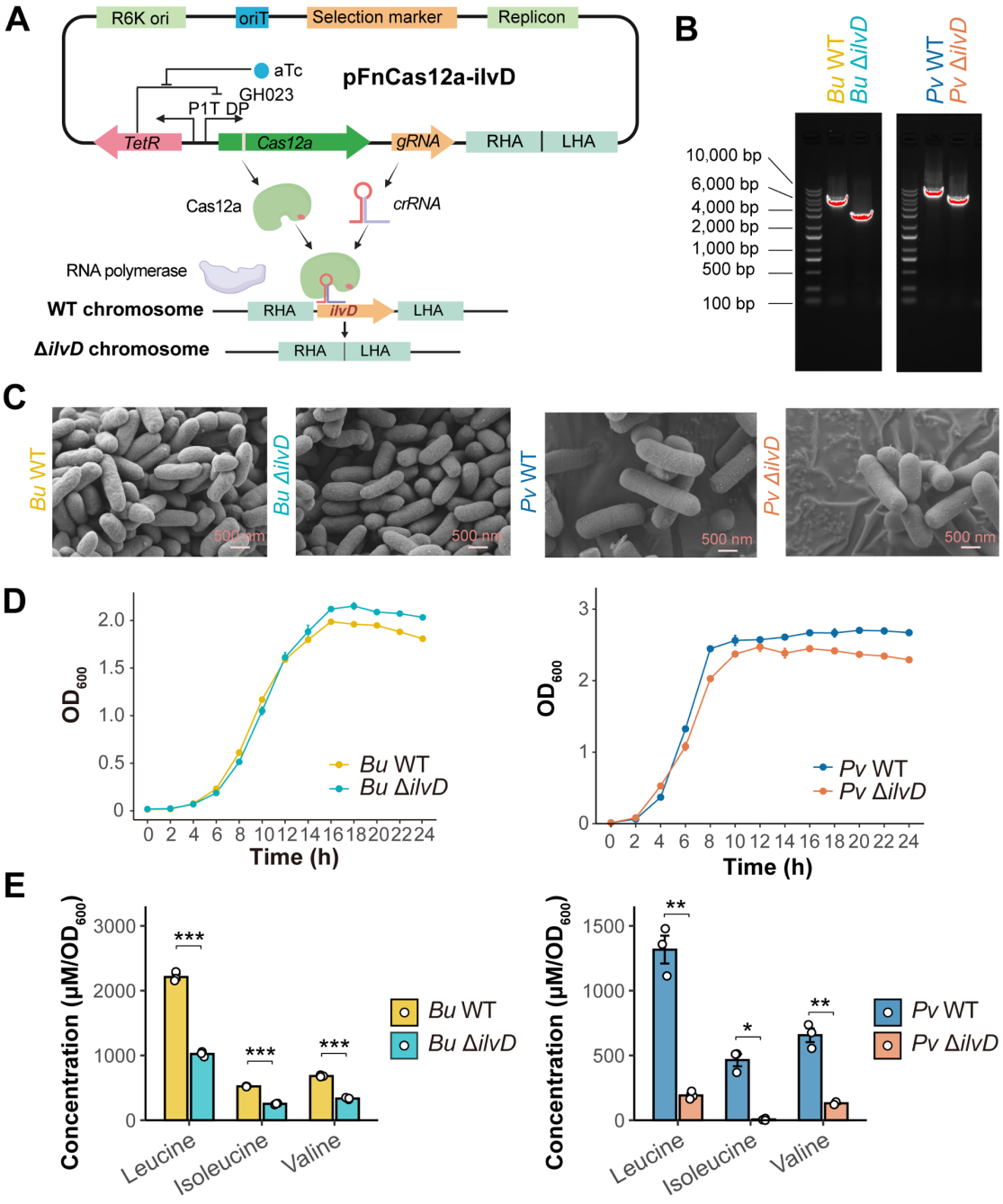


Figure 2. Deletion of *ilvD* reduces BCAA production in representative gut bacteria.
(A) Schematic illustration of CRISPR-Cas12a-mediated *ilvD* deletion. The engineered plasmid encodes an anhydrotetracycline (aTc)-inducible Cas12a, a guide RNA targeting *ilvD* and flanking homology arms (RHA/LHA) for homologous recombination.
(B) PCR validation of *ilvD* deletion in *B. uniformis* and *P. vulgatus*. The expected amplicon size shifts confirm successful *ilvD* knockout (Δ*ilvD*) in both species relative to their WT counterparts.
(C) Representative scanning electron microscopy images of WT and Δ*ilvD* strains. Scale bars, 500 nm.

Langtaosha (LTS) Preprint doi: https://doi.org/10.65215/LTSpreprints.2026.11.27.000404. This version posted November 27, 2026. The copyright holder for this preprint (which was not certified by peer review) is the author/funder. Creative Commons license: CC Attribution-NonCommercial-NoDerivatives 4.0 https://creativecommons.org/licenses/by-nc-nd/4.0

(D) Growth kinetics of WT and Δ*ilvD* strains of *B. uniformis* and *P. vulgatus* over 24 h (n = 3 bacterial cultures per group).
(E) Extracellular concentrations of leucine, isoleucine, and valine in cultures of WT and Δ*ilvD* strains of *B. uniformis* and *P. vulgatus*, normalized to OD_{600} (n = 3 bacterial cultures per group). Data are presented as mean ± SD in (D) and mean ± SEM in (E). In (E), statistical significance was determined using two-sided Welch's *t*-tests, with Holm correction for multiple comparisons. *p < 0.05; **p < 0.01; ***p < 0.001.

Genetic disruption of microbial BCAA biosynthesis improves host insulin sensitivity

To determine the contribution of microbial BCAA biosynthesis to host insulin sensitivity, we performed monocolonization experiments in two complementary mouse models: germ-free mice and antibiotic-pretreated specific-pathogen-free (SPF) mice with depleted endogenous microbiota (Figures 3A). Mice were colonized with either *Bu* WT or *Bu* Δ*ilvD* and maintained on a normal chow diet (NCD). *Bu* WT and *Bu* Δ*ilvD* achieved comparable colonization levels in both mouse models (Figures 3B). Mice colonized with *Bu* Δ*ilvD* strains showed improved glucose tolerance and insulin sensitivity relative to their WT-colonized counterparts, as assessed by oral glucose tolerance tests (OGTTs) and insulin tolerance tests (ITTs) (Figures 3C–3F). Consistent with reduced microbial BCAA production, *Bu* Δ*ilvD*-colonized mice had significantly lower fecal and circulating BCAA levels (Figures 3G-H). In further support of these findings, we tested a *Pv* Δ*ilvD* strain in antibiotic-pretreated SPF mice and observed comparable colonization levels, similar improvements in glucose tolerance and insulin sensitivity, and reductions in fecal and circulating BCAA levels (Figure S5). Together, these results provide genetic evidence from two bacterial species that microbial BCAA biosynthesis contributes to impaired host insulin sensitivity in mice.

We next examined whether the metabolic effects of disrupting microbial BCAA biosynthesis were maintained across different dietary conditions. Antibiotic-treated SPF mice were colonized with WT or *Bu* Δ*ilvD* and maintained on NCD, an inulin-enriched diet (IED), or a high-fat diet (HFD) (Figure S6A). WT and *Bu* Δ*ilvD* achieved comparable colonization levels under each dietary condition (Figure S6B), whereas *Bu* Δ*ilvD* colonization consistently improved glucose tolerance and insulin sensitivity relative to WT colonization (Figures 3E, 3F, S6C, and S6D). These results indicate that the metabolic effects associated with disruption of microbial BCAA biosynthesis are maintained across the dietary conditions examined.

We further examined inflammatory responses and insulin signaling in *Bu* WT- and Δ*ilvD*-colonized mice. Serum concentrations of the pro-inflammatory cytokines TNF-α and IL-6 were reduced in *Bu* Δ*ilvD*-colonized mice, together with decreased expression of inflammatory mediators in the liver, skeletal muscle, and epididymal white adipose tissue

Langtaosha (LTS) Preprint doi: https://doi.org/10.65215/LTSpreprints.2026.11.27.000404. This version posted November 27, 2026. The copyright holder for this preprint (which was not certified by peer review) is the author/funder. Creative Commons license: CC Attribution-NonCommercial-NoDerivatives 4.0 https://creativecommons.org/licenses/by-nc-nd/4.0

(eWAT) (Figures 3I and S7). Akt phosphorylation at Ser473 was increased in the liver and eWAT of *Bu* Δ*ilvD*-colonized mice (Figures 3J and S8), consistent with enhanced insulin signaling. Together, these findings show that improved insulin sensitivity following disruption of microbial BCAA biosynthesis is accompanied by reduced inflammatory responses and enhanced insulin signaling.

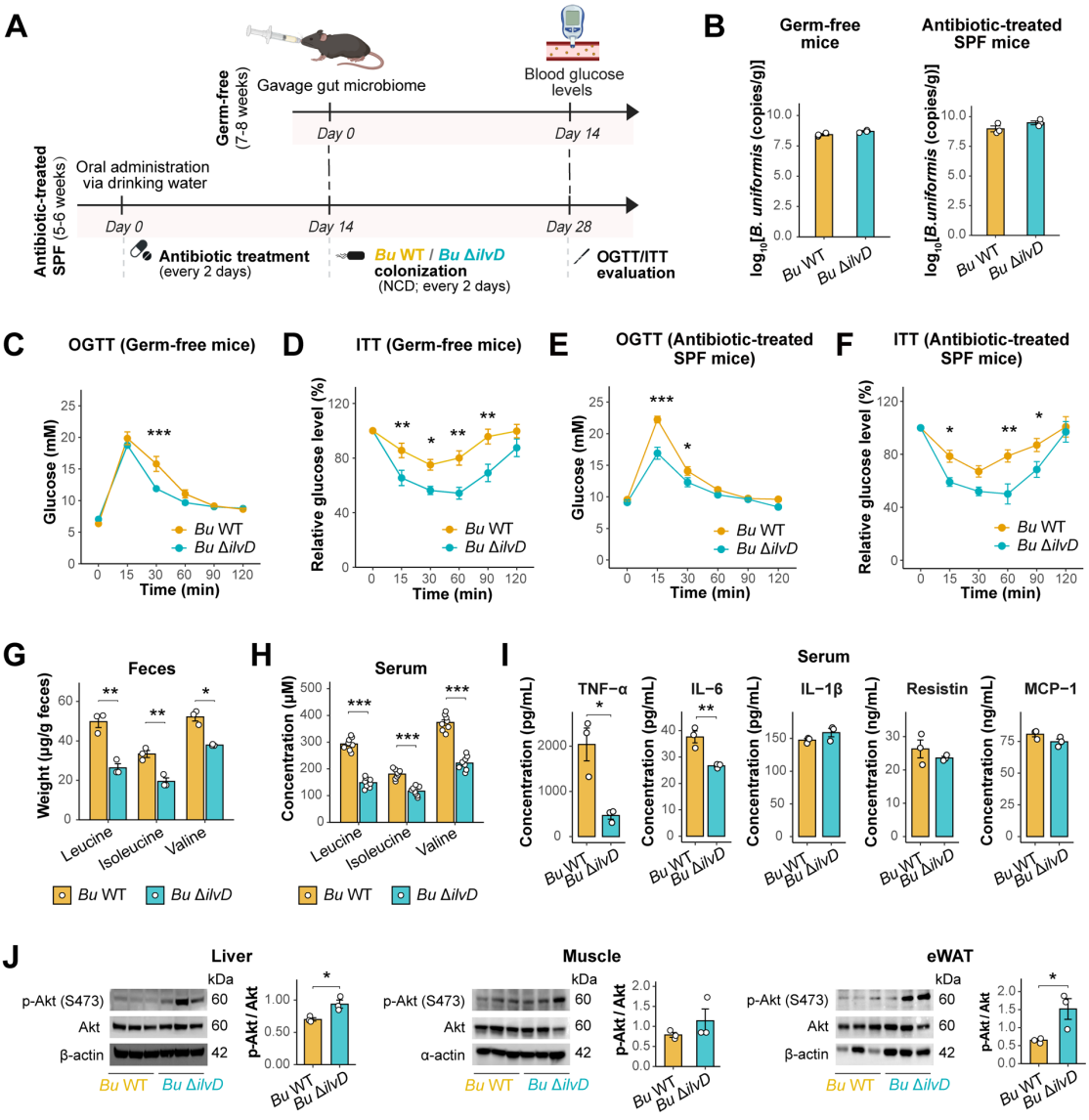


Figure 3. Genetic disruption of gut microbial BCAA biosynthesis improves glucose homeostasis and insulin sensitivity in mice.

(A) Schematic of the experimental design. Germ-free mice were orally colonized with *B. uniformis* (*Bu*) WT or *Bu* Δ*ilvD* for 14 days. Antibiotic-treated SPF mice received antibiotics for 14 days, followed by oral colonization with *Bu* WT or *Bu* Δ*ilvD* for 14 days while maintained on a normal chow diet (NCD).

(B) Fecal abundance of *Bu* WT and *Bu* Δ*ilvD* in germ-free and antibiotic-treated SPF mice at the experimental endpoint, quantified by qPCR.

(C and D) Oral glucose tolerance test (OGTT) (C) and insulin tolerance test (ITT) (D) in germ-free mice colonized with *Bu* WT or *Bu* Δ*ilvD*.

Langtaosha (LTS) Preprint doi: https://doi.org/10.65215/LTSpreprints.2026.11.27.000404. This version posted November 27, 2026. The copyright holder for this preprint (which was not certified by peer review) is the author/funder. Creative Commons license: CC Attribution-NonCommercial-NoDerivatives 4.0 https://creativecommons.org/licenses/by-nc-nd/4.0

(E and F) OGTT and ITT in antibiotic-treated SPF mice colonized with *Bu* WT or *Bu* Δ*ilvD* (*n* = 8 mice per group).
(G and H) Fecal (G) and serum (H) concentrations of leucine, isoleucine, and valine in germ-free mice colonized with *Bu* WT or *Bu* Δ*ilvD* (*n* = 3 mice per group for feces; *n* = 8 mice per group for serum).
(I) Serum concentrations of TNF-α, IL-6, IL-1β, resistin, and MCP-1 in germ-free mice colonized with *Bu* WT or *Bu* Δ*ilvD* (*n* = 3 mice per group).
(J) Representative western blots (left) and densitometric quantification (right) of Akt phosphorylation at Ser473 in the liver, skeletal muscle, and epididymal white adipose tissue (eWAT) of germ-free mice colonized with *Bu* WT or *Bu* Δ*ilvD* (*n* = 3 mice per group). p-Akt levels were normalized to total Akt.
Data are presented as mean ± SEM. Statistical significance was assessed using two-sided Welch's *t*-tests in (B), (I), and (J); two-way repeated-measures ANOVA followed by least significant difference (LSD) post hoc tests in (C)–(F); and two-sided Welch's *t*-tests with Holm correction for multiple comparisons in (G) and (H). **p* < 0.05; ***p* < 0.01; ****p* < 0.001.

BCAA biosynthesis is broadly distributed and DHAD is conserved across human gut bacteria

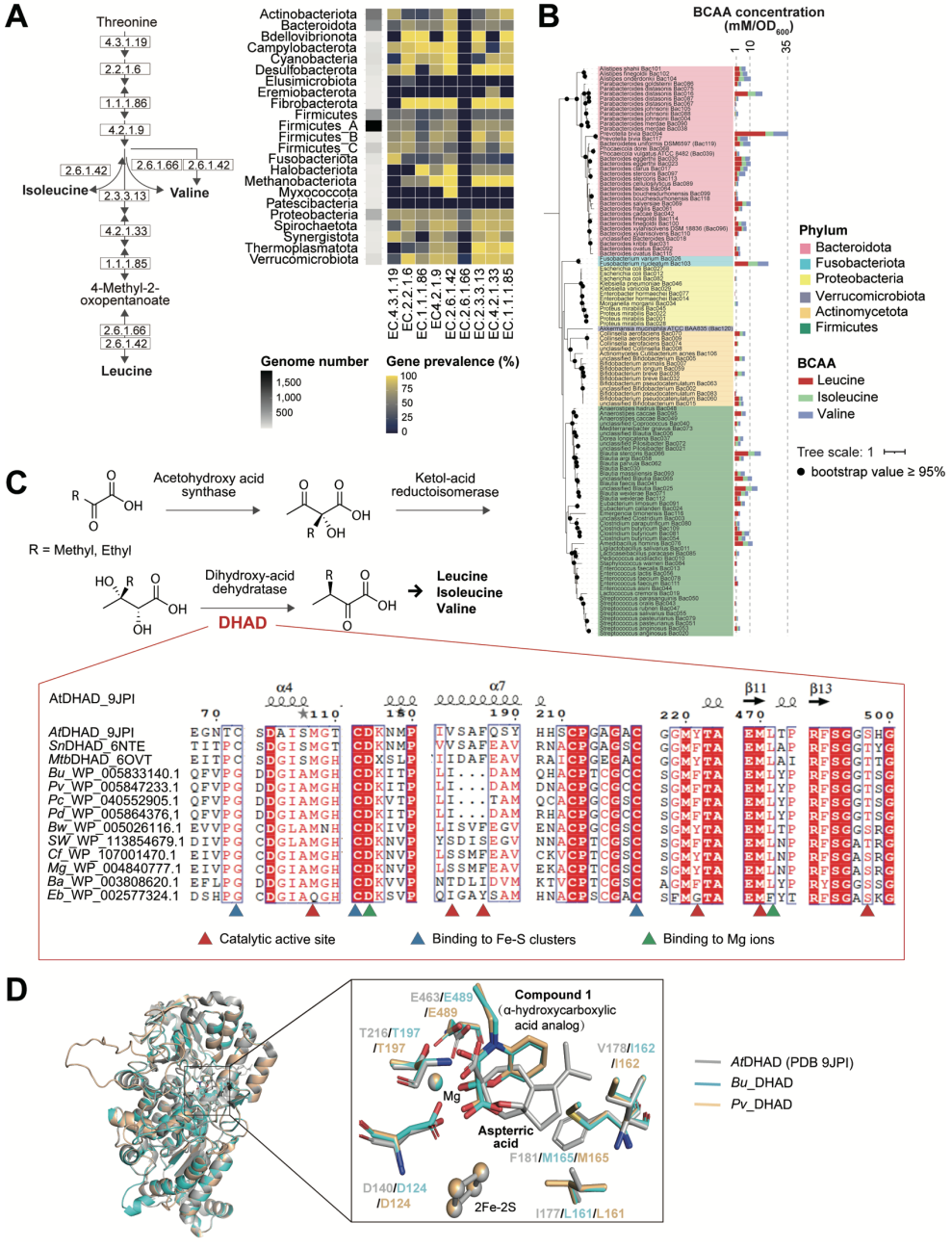
To determine the distribution of BCAA biosynthetic capacity across human gut bacteria, we performed a large-scale pan-genomic analysis of 204,938 gut microbial genomes spanning 20 major taxonomic classes (Figure S9A). Pathway annotation of 4,789 representative genomes and MAGs showed that BCAA biosynthetic genes are broadly distributed across major gut bacterial phyla (Figure 4A). Similar patterns were observed across geographically and demographically distinct human cohorts, indicating that BCAA biosynthetic capacity is broadly represented among the human gut bacterial genomes examined (Figures S9B and S10).

To experimentally assess BCAA production across phylogenetically diverse gut bacteria, we cultured 114 representative human gut bacterial isolates under strict anaerobic conditions in BHI medium. BCAA production was detected across phylogenetically diverse bacterial phyla, including Bacteroidota, Bacillota, and Actinobacteriota, with members of the genera *Bacteroides*, *Parabacteroides*, *Prevotella*, *Fusobacterium*, *Collinsella*, *Blautia*, and *Clostridium* producing relatively high levels of BCAAs (Figure 4B and Table S5). These results provide experimental support for the broad distribution of BCAA-producing capacity across phylogenetically diverse gut bacteria.

Because mammals lack the BCAA biosynthetic pathway and DHAD has previously been explored as a target of herbicides,[30,31] we next examined the sequence and structural conservation of DHAD across gut bacteria. Multiple-sequence alignment of DHAD orthologs from ten major gut bacterial phyla, together with three DHAD proteins with experimentally resolved crystal structures, revealed substantial conservation of residues

Langtaosha (LTS) Preprint doi: https://doi.org/10.65215/LTSpreprints.2026.11.27.000404. This version posted November 27, 2026. The copyright holder for this preprint (which was not certified by peer review) is the author/funder. Creative Commons license: CC Attribution-NonCommercial-NoDerivatives 4.0 https://creativecommons.org/licenses/by-nc-nd/4.0

involved in catalysis, Fe–S cluster coordination, and Mg^{2+} binding (Figure 4C). Structural superposition of predicted DHAD structures from the two representative BCAA-producing species, *B. uniformis* (*Bu*_DHAD) and *P. vulgatus* (*Pv*_DHAD), and eight additional gut microbial DHADs with three experimentally determined DHAD structures revealed a highly conserved active-site architecture (Figure 4D). Structural comparisons across the examined gut bacterial DHAD orthologs yielded root-mean-square deviation (RMSD) values of 1.039–1.473 Å (Figure S11). Together, the sequence and structural conservation of DHAD, particularly its active-site architecture, provides a rationale for testing whether DHAD inhibitors, including α-hydroxycarboxylic acid analogs [31,32] and aspterric acid [30] (Figure 4D), can inhibit BCAA biosynthesis across diverse gut bacteria .



Langtaosha (LTS) Preprint doi: https://doi.org/10.65215/LTSpreprints.2026.11.27.000404. This version posted November 27, 2026. The copyright holder for this preprint (which was not certified by peer review) is the author/funder. Creative Commons license: CC Attribution-NonCommercial-NoDerivatives 4.0 https://creativecommons.org/licenses/by-nc-nd/4.0

Figure 4. BCAA biosynthetic capacity is broadly distributed and DHAD is conserved across human gut bacteria.

(A) Prevalence of BCAA biosynthetic genes across 4,789 representative gut bacterial genomes and MAGs. Left, schematic of the BCAA biosynthetic pathway; right, heatmap showing the prevalence of BCAA biosynthetic genes across major gut bacterial phyla.

(B) Phylogenetic distribution of BCAA production across 114 cultured human gut bacterial isolates. The maximum-likelihood phylogenetic tree (TIM3e+I+G4 model) is colored by phylum, with adjacent bar plots showing culture supernatant concentrations of leucine, isoleucine, and valine normalized to OD600.

(C) Sequence conservation of DHAD across phylogenetically diverse gut bacteria. Multiple-sequence alignment includes DHAD orthologs from representative gut bacteria together with structurally characterized DHAD proteins from *Arabidopsis thaliana* (*At*DHAD, PDB: 9JPI), *Synechocystis* sp. PCC 6803 (*Sn*DHAD, PDB: 6NTE), and *Mycobacterium tuberculosis* (*Mtb*DHAD, PDB: 6OVT). Conserved residues involved in catalysis, Fe–S cluster coordination, and Mg^{2+} binding are indicated.

(D) Structural superposition of predicted *Bu*_DHAD and *Pv*_DHAD) structures with *At*DHAD (PDB: 9JPI). The enlarged view highlights the conserved active-site architecture, including the 2Fe–2S cluster, Mg^{2+} ion, and residues involved in substrate binding and catalysis. The binding poses of the known DHAD inhibitors Compound 1 (formerly I-6e[31]) and aspterric acid[30] are shown within the active site. Protein structures are color-coded as indicated.

Identification of small-molecule inhibitors of gut microbial DHADs

Building on the structural conservation of microbial DHADs and the absence of its functional ortholog in mammals,[30] we sought to identify small-molecule inhibitors of gut microbial DHADs. We screened an in-house library of 27 α-hydroxycarboxylic acid derivatives previously developed by our group,[31] together with aspterric acid,[30] a reported DHAD inhibitor.

We recombinantly expressed and purified DHAD orthologs from two representative T2DM-enriched, BCAA-producing species, *B. uniformis* and *P. vulgatus*. Biochemical screening identified multiple compounds with inhibitory activity against *Bu*_DHAD and *Pv*_DHAD (Figures 5A, S12A–S12B). Among these, Compound 1 (7-fluoro-2-hydroxy-3-oxo-4-propyne-3,4-dihydro-2H-benzo[b][1,4]oxazine-2-carboxylic acid) and Compound 2 (7-fluoro-2-hydroxy-4-(3-methylbut-2-en-1-yl)-3-oxo-3,4-dihydro-2H-benzo[b][1,4]oxazine-2-carboxylic acid) were selected for further characterization. Dose–response assays against *Bu*_DHAD yielded half-maximal inhibitory concentration (IC50) values of 67.0 μM for Compound 1 and 22.1 μM for Compound 2 (Figure S12C). At 100 μM, Compound 1 inhibited *Bu*_DHAD and *Pv*_DHAD by 69.6% and 67.2%, respectively, whereas Compound 2 inhibited the two enzymes by 54.9% and 44.2%, respectively (Figure 5A).

We next evaluated the activity of Compounds 1 and 2 against eight purified DHAD orthologs from four bacterial phyla. Both compounds inhibited multiple DHAD orthologs,

Langtaosha (LTS) Preprint doi: https://doi.org/10.65215/LTSpreprints.2026.11.27.000404. This version posted November 27, 2026. The copyright holder for this preprint (which was not certified by peer review) is the author/funder. Creative Commons license: CC Attribution-NonCommercial-NoDerivatives 4.0 https://creativecommons.org/licenses/by-nc-nd/4.0

although the magnitude of inhibition varied across the enzymes examined (Figure 5B). Compound 1 was selected for further characterization and reduced extracellular leucine, isoleucine, and valine levels in *B. uniformis* cultures (Figure 5C). Surface plasmon resonance (SPR) analysis further showed direct binding of Compound 1 to both *Bu*_DHAD (*K*D = 10.9 μM) and *Pv*_DHAD (*K*D = 26.6 μM) (Figure 5D), consistent with its biochemical inhibitory activity. Neither Compound 1 nor Compound 2 caused substantial loss of viability in Caco-2, HepG2, or HEK-293 cells over the tested concentration range of 0.01–1,000 μM, with cell viability remaining above 80% under the conditions examined (Figure S13).

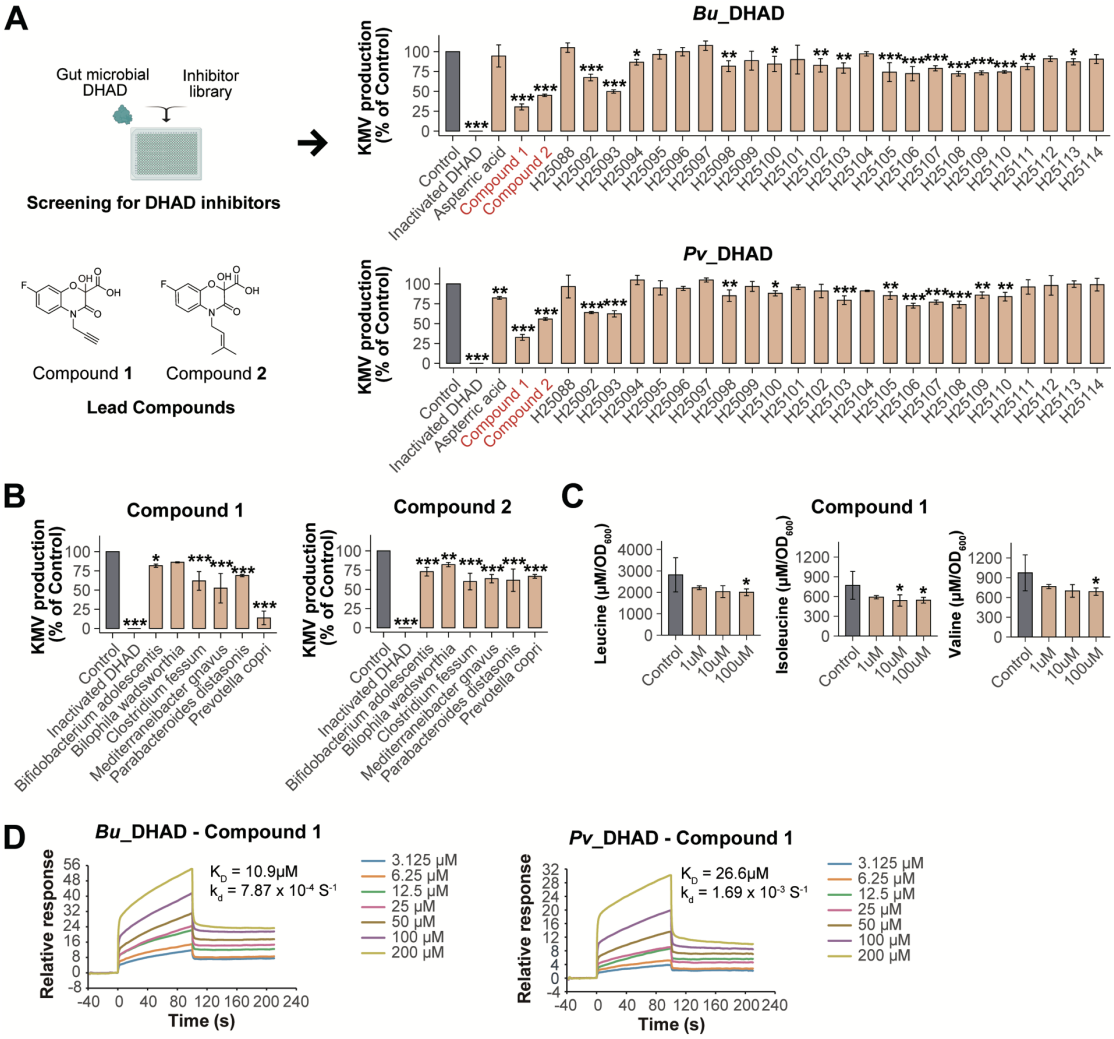


Figure 5. Identification and characterization of inhibitors of gut microbial DHADs.

(A) Screening of a chemical library for inhibitors of *B. uniformis* DHAD (*Bu*_DHAD; top) and *P. vulgatus* DHAD (*Pv*_DHAD; bottom). Enzymatic activity was assessed by LC-MS quantification of 2-keto-3-methylvalerate (KMV) production and is shown relative to the vehicle control. Left, schematic of the screening workflow and chemical structures of Compound 1 and Compound 2. Heat-inactivated DHAD was included as a negative control.

(B) Inhibitory activity of Compound 1 (left) and Compound 2 (right) against purified DHAD orthologs from representative gut bacteria (*n* = 3 independent enzymatic reactions per group). The strategy for selecting bacterial DHAD orthologs is detailed in Figure S11. Orthologs without detectable enzymatic activity under the assay conditions were excluded from analysis.

Langtaosha (LTS) Preprint doi: https://doi.org/10.65215/LTSpreprints.2026.11.27.000404. This version posted November 27, 2026. The copyright holder for this preprint (which was not certified by peer review) is the author/funder. Creative Commons license: CC Attribution-NonCommercial-NoDerivatives 4.0 https://creativecommons.org/licenses/by-nc-nd/4.0

(C) Extracellular concentrations of leucine, isoleucine, and valine in *B. uniformis* cultures treated with the indicated concentrations of Compound 1, normalized to OD600 (n = 3 bacterial cultures per group).
(D) Surface plasmon resonance sensorgrams showing binding of Compound 1 to recombinant *Bu*_DHAD (left) and *Pv*_DHAD (right). Equilibrium dissociation constants (K_D) and dissociation rate constants (k_d) are indicated.
Data are presented as mean ± SD. Statistical significance was determined using two-sided Welch's t-tests. *$p < 0.05$; **$p < 0.01$; ***$p < 0.001$.

Gut microbial DHAD inhibition improves insulin sensitivity in diet-induced obesity

To assess the *in vivo* metabolic effects of DHAD inhibitors, we first examined whether Compounds 1 and 2 acutely affected host glucose homeostasis. OGTT and ITT performed 30 min after a single oral administration showed no significant changes in glucose tolerance or insulin sensitivity in SPF mice (Figure S14).

We next evaluated Compound 1 in NCD-fed mice and diet-induced obese (DIO) mice following 14 days of daily oral administration (Figure 6A). In NCD-fed mice, Compound 1 reduced fecal and circulating BCAA concentrations and improved insulin sensitivity without significantly affecting glucose tolerance (Figures 6B–6D). In DIO mice, Compound 1 improved both glucose tolerance and insulin sensitivity relative to vehicle-treated controls after 7 and 14 days of treatment (Figures 6B and S15A). These changes were accompanied by reductions in fecal and circulating BCAA levels (Figures 6C, 6D, and S15B).

16S rRNA gene sequencing revealed no significant differences in alpha diversity or overall community structure (Bray–Curtis PCoA) between treatment and control groups, with limited changes in the relative abundance of dominant genera (Figures 6E, 6F, and S15C), suggesting that Compound 1 did not broadly alter gut microbial community structure under the tested conditions. Parallel tolerability assessments showed no significant changes in the measured intestinal, hepatic, or renal parameters. Compound 1 treatment did not significantly alter colon length in either NCD-fed or DIO mice (Figure S15D), histological evaluation by hematoxylin and eosin staining showed no significant differences in colon injury scores between treatment and control groups (Figure S15E). Serum markers of hepatic and renal function, including alanine aminotransferase (ALT), aspartate aminotransferase (AST), and creatinine (Cr), also remained comparable between treatment and control groups (Figure 6G). Together, these findings show that 14-day Compound 1 treatment reduced fecal and circulating BCAA levels and improved insulin sensitivity without broad alterations in gut microbial community structure or detectable changes in the intestinal, hepatic, and renal parameters assessed.

Langtaosha (LTS) Preprint doi: https://doi.org/10.65215/LTSpreprints.2026.11.27.000404. This version posted November 27, 2026. The copyright holder for this preprint (which was not certified by peer review) is the author/funder. Creative Commons license: CC Attribution-NonCommercial-NoDerivatives 4.0 https://creativecommons.org/licenses/by-nc-nd/4.0

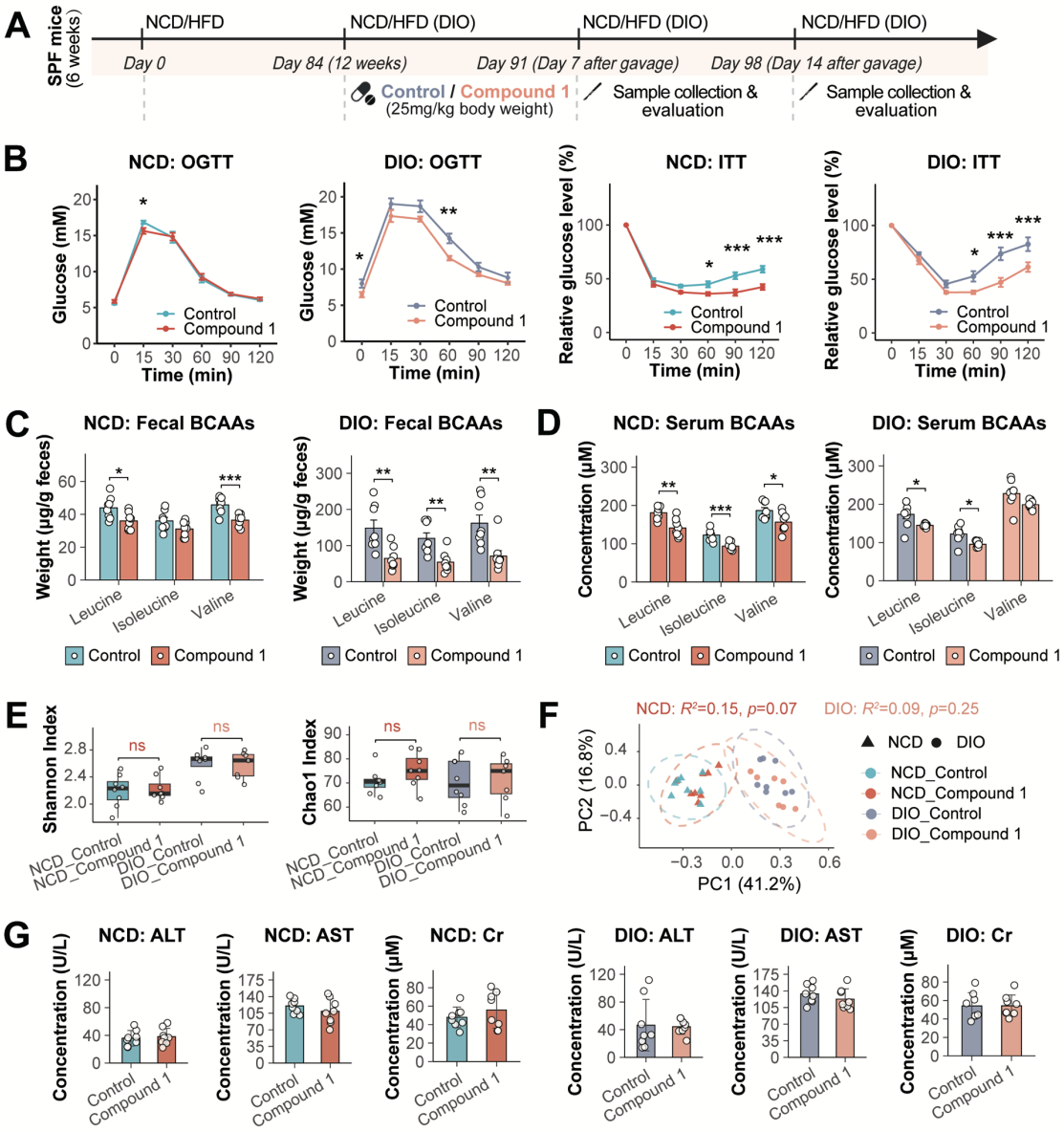


Figure 6. DHAD inhibition reduces BCAA levels and improves insulin sensitivity in diet-induced obese mice without broadly altering gut microbial community structure.

(A) Schematic of the experimental design. Six-week-old SPF mice were maintained on a normal chow diet (NCD) or high-fat diet (HFD) for 12 weeks. Mice then received daily oral gavage of vehicle control (0.5% DMSO) or Compound 1 (25 mg/kg body weight) for 14 days. Phenotypic assessments and sample collection were performed on days 7 and 14 after treatment initiation.

(B) OGTTs and ITTs in NCD-fed and diet-induced obese (DIO) mice following 14 days of Compound 1 or vehicle (0.5% DMSO) treatment (n = 8 mice per group).

(C and D) Fecal (C) and serum (D) concentrations of leucine, isoleucine, and valine in NCD-fed and DIO mice following 14 days of Compound 1 or vehicle (0.5% DMSO) treatment (n = 8 mice per group).

(E) Alpha diversity of the fecal microbiota, assessed using the Shannon and Chao1 indices, in NCD-fed and DIO mice after 14 days of treatment (n = 8 mice per group).

Langtaosha (LTS) Preprint doi: https://doi.org/10.65215/LTSpreprints.2026.11.27.000404. This version posted November 27, 2026. The copyright holder for this preprint (which was not certified by peer review) is the author/funder. Creative Commons license: CC Attribution-NonCommercial-NoDerivatives 4.0 https://creativecommons.org/licenses/by-nc-nd/4.0

(F) Principal coordinate analysis (PCoA) of fecal microbial communities based on Bray–Curtis dissimilarity at the genus level in NCD-fed and DIO mice after 14 days of treatment (n = 8 mice per group).
(G) Serum alanine aminotransferase (ALT), aspartate aminotransferase (AST), and creatinine (Cr) levels in NCD-fed and DIO mice after 14 days of treatment (n = 8 mice per group).
Data in (B), (C), (D), and (G) are presented as mean ± SEM. Statistical significance was assessed by two-way repeated-measures ANOVA followed by LSD post hoc tests in (B); two-sided Wilcoxon rank-sum tests with Holm correction for multiple comparisons in (C)–(E); PERMANOVA with Holm correction for pre-specified pairwise comparisons in (F); and two-sided Welch's t-tests in (G). *$p < 0.05$; **$p < 0.01$; ***$p < 0.001$.

We further evaluated Compound 1 in *db/db* mice, a leptin receptor-deficient genetic model of severe obesity, insulin resistance, and hyperglycemia (Figure S16A). In WT littermates, Compound 1 improved insulin sensitivity and reduced fasting blood glucose after 7 and 14 days of treatment, accompanied by reductions in fecal BCAA levels and, at day 14, circulating leucine (Figures S16B–S16F). In contrast, Compound 1 did not significantly alter insulin sensitivity or fasting blood glucose in *db/db* mice at either time point (Figures S16B and S16C). Despite significant reductions in fecal leucine, isoleucine, and valine after treatment, circulating BCAA levels remained unchanged in *db/db* mice (Figures S16D–S16F). Together, these results show that the metabolic response to Compound 1 differs between WT and *db/db* mice and that reductions in fecal BCAA levels in *db/db* mice are not accompanied by corresponding reductions in circulating BCAA levels or improvements in insulin sensitivity.

Gut microbial BCAA production is associated with T2DM in human cohorts

To evaluate the clinical relevance of gut microbial BCAA production in T2DM, we analyzed fecal samples from an independent cohort of 100 participants, including 50 individuals with T2DM and 50 healthy controls (Figure 7A). Targeted metabolomic analysis showed that fecal concentrations of total BCAAs, as well as leucine, isoleucine, and valine individually, were significantly higher in individuals with T2DM than in healthy controls (Figure 7B). Probe-based qPCR further showed higher fecal abundances of *B. uniformis* and *P. vulgatus*, two BCAA-producing species identified in our analyses, in individuals with T2DM (Figures 7C and 7D). The fecal abundances of both species were positively correlated with fecal concentrations of leucine, isoleucine, and valine (Figures 7E and 7F), further linking the abundance of these BCAA-producing bacteria with fecal BCAA levels in this cohort.

We next examined BCAA biosynthetic genes in multiple public fecal metagenomic cohorts. Core BCAA biosynthetic genes, including *ilvD* and *ilvE*, were significantly more abundant in individuals with T2DM than in healthy controls (Figure S17), providing independent evidence for increased microbial genetic capacity for BCAA biosynthesis in

Langtaosha (LTS) Preprint doi: https://doi.org/10.65215/LTSpreprints.2026.11.27.000404. This version posted November 27, 2026. The copyright holder for this preprint (which was not certified by peer review) is the author/funder. Creative Commons license: CC Attribution-NonCommercial-NoDerivatives 4.0 https://creativecommons.org/licenses/by-nc-nd/4.0

T2DM-associated gut microbiomes. Together, these data demonstrate consistent associations among BCAA-producing bacteria, microbial BCAA biosynthetic capacity, and T2DM across the human cohorts examined.

Finally, we evaluated the discriminatory performance of the Cluster A microbial signature identified above across a combined dataset of 1,251 human gut metagenomes. The signature distinguished healthy individuals from those with obesity, polycystic ovary syndrome (PCOS), non-alcoholic fatty liver disease (NAFLD), atherosclerotic cardiovascular disease (ASCVD), or T2DM, with AUC values ranging from 0.70 to 0.93 (Figure 7G). These results show that the T2DM-associated microbial signature identified in our initial analysis is also associated with multiple metabolic disorders characterized by insulin resistance.

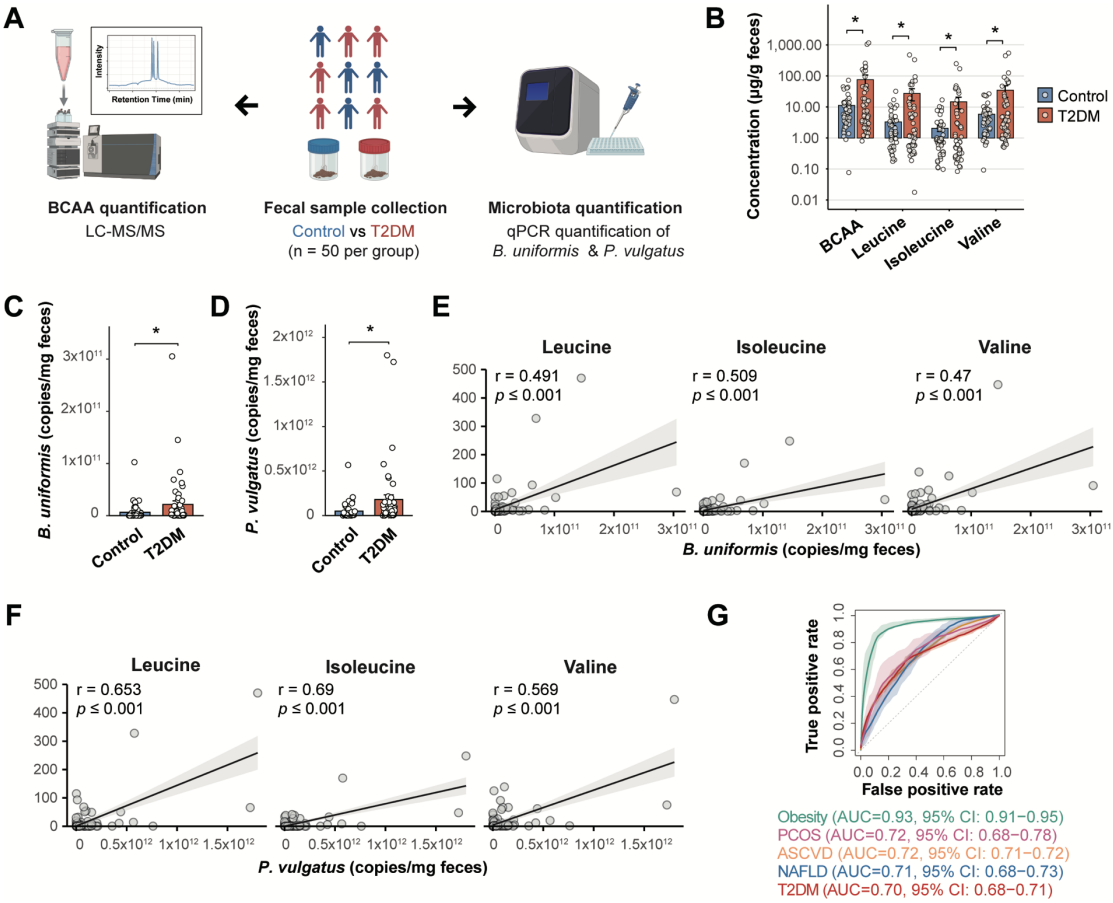


Figure 7. Fecal BCAA levels and BCAA-producing bacteria are elevated in T2DM and associated with metabolic disease across human cohorts.

(A) Schematic of the clinical cohort study design. A total of 100 participants, including 50 individuals with T2DM and 50 healthy controls, were enrolled for fecal BCAA quantification and bacterial load analysis.

(B) Fecal concentrations of total BCAAs, leucine, isoleucine, and valine in individuals with T2DM and healthy controls (n = 50 per group).

(C and D) Fecal loads of *B. uniformis* (C) and *P. vulgatus* (D) in individuals with T2DM and healthy controls, quantified by probe-based qPCR (n = 50 per group).

Langtaosha (LTS) Preprint doi: https://doi.org/10.65215/LTSpreprints.2026.11.27.000404. This version posted November 27, 2026. The copyright holder for this preprint (which was not certified by peer review) is the author/funder. Creative Commons license: CC Attribution-NonCommercial-NoDerivatives 4.0 https://creativecommons.org/licenses/by-nc-nd/4.0

(E and F) Spearman's correlations between fecal loads of *B. uniformis* (E) or *P. vulgatus* (F) and fecal concentrations of leucine, isoleucine, and valine. Spearman's correlation coefficients (*r*) and corresponding *P* values are indicated.

(G) Receiver operating characteristic (ROC) curves evaluating the discriminatory performance of the Cluster A microbial signature for T2DM and four additional metabolic disorders associated with insulin resistance: obesity, polycystic ovary syndrome (PCOS), non-alcoholic fatty liver disease (NAFLD), and atherosclerotic cardiovascular disease (ASCVD). AUC values and 95% confidence intervals are indicated for each disease.

Data in (B)–(D) are presented as mean ± SEM. Statistical significance was assessed using two-sided Welch's *t*-tests with Holm correction for multiple comparisons in (B) and two-sided Welch's *t*-tests in (C) and (D). Correlations in (E) and (F) were assessed using two-sided Spearman's rank correlation tests. *$p < 0.05$; **$p < 0.01$; ***$p < 0.001$.

Discussion

Our study identifies gut microbial *de novo* BCAA biosynthesis as a contributor to IR and provides genetic and pharmacological evidence supporting the conserved microbial enzyme DHAD as a candidate target for microbiota-directed intervention. Although elevated circulating BCAAs have long been linked to IR, previous studies have primarily focused on dietary BCAA intake,[12,13] host BCAA metabolism,[14] or microbial BCAA utilization.[15,16] By integrating human microbiome multi-omics, microbial genetics, complementary mouse models, comparative genomic and structural analyses, and small-molecule inhibition, we show that gut microbial BCAA biosynthesis contributes to impaired insulin sensitivity in the experimental models examined and establish the feasibility of pharmacologically targeting this microbial pathway. Together, these findings provide a rationale for further investigating microbial BCAA biosynthesis as a potential intervention point in IR-associated metabolic disease.

Previous metagenomic studies have associated multiple microbiota-derived amino acid metabolites, including BCAAs, imidazole propionate, and aromatic amino acid derivatives, with impaired insulin sensitivity.[6,10,15,29] However, the relative contributions of different microbial amino acid metabolic pathways to IR remain incompletely understood.[6,33,34] By systematically profiling major microbial amino acid metabolic pathways at both metagenomic and metatranscriptomic levels, we identified enrichment of BCAA biosynthetic genes and transcripts in T2DM-associated microbial communities. This association was further supported in independent human cohorts by increased fecal BCAA levels, enrichment of representative BCAA-producing species, and increased abundance of core BCAA biosynthetic genes. In addition, the T2DM-associated Cluster A microbial signature showed discriminatory capacity across several metabolic disorders associated with IR.

Although genetic validation was performed in representative T2DM-enriched strains,

Langtaosha (LTS) Preprint doi: https://doi.org/10.65215/LTSpreprints.2026.11.27.000404. This version posted November 27, 2026. The copyright holder for this preprint (which was not certified by peer review) is the author/funder. Creative Commons license: CC Attribution-NonCommercial-NoDerivatives 4.0 https://creativecommons.org/licenses/by-nc-nd/4.0

our findings extend well beyond individual bacterial species. Comparative genomic analysis showed that BCAA biosynthetic genes are broadly distributed across phylogenetically diverse gut bacteria, while experimental analysis of more than 100 gut bacterial isolates demonstrated BCAA production across multiple bacterial phyla. Sequence comparisons and structural modeling further supported substantial conservation of DHAD, particularly its active-site architecture, across the bacterial orthologs examined. Thus, *B. uniformis* and *P. vulgatus* provide genetically tractable models for studying a metabolic function that is distributed across diverse members of the gut microbiota, rather than representing the only taxa relevant to this pathway. This broad distribution has potential therapeutic implications: targeting a conserved metabolic enzyme such as DHAD could, in principle, modulate BCAA production across multiple gut bacterial species without requiring species-specific depletion.

Our study further provides a rationale for targeting microbial BCAA biosynthesis rather than directly manipulating host BCAA metabolism. Although elevated circulating BCAAs are strongly associated with IR,[10,35] therapeutic strategies have largely focused on host BCAA catabolism.[14-16] DHAD is particularly attractive in this context because the BCAA biosynthetic pathway is absent in mammals and has previously been targeted for herbicidal and antimicrobial applications.[30,36] Compound 1 inhibited DHAD orthologs from multiple gut bacterial species, reduced BCAA production by *B. uniformis in vitro*, and lowered fecal and circulating BCAA levels in treated mice. Notably, treatment did not broadly alter gut microbial diversity or community structure under the conditions examined, suggesting that modulation of microbial metabolic activity can occur without major disruption of community composition. These findings support microbial DHAD inhibition as a strategy for modulating BCAA production, although the microbial and host selectivity of the current compounds will require further characterization.

The effects of Compound 1 also differed across metabolic models. In diet-induced obese mice, Compound 1 reduced fecal and circulating BCAA levels and improved glucose tolerance and insulin sensitivity. In contrast, in *db/db* mice, a leptin receptor-deficient genetic model of obesity and diabetes, Compound 1 reduced fecal BCAA levels but did not significantly reduce circulating BCAA levels or improve insulin sensitivity. This dissociation indicates that reducing fecal BCAA levels does not necessarily coincide with reduced systemic BCAA levels or improved insulin sensitivity across different metabolic backgrounds. The lack of efficacy in *db/db* mice may reflect differences in the relative contribution of microbial BCAA metabolism to systemic metabolic dysfunction in genetically driven versus diet-induced disease, although the underlying mechanisms remain to be determined. These findings therefore define an important boundary of the observed pharmacological effect and suggest that the metabolic consequences of targeting microbial

Langtaosha (LTS) Preprint doi: https://doi.org/10.65215/LTSpreprints.2026.11.27.000404. This version posted November 27, 2026. The copyright holder for this preprint (which was not certified by peer review) is the author/funder. Creative Commons license: CC Attribution-NonCommercial-NoDerivatives 4.0 https://creativecommons.org/licenses/by-nc-nd/4.0

BCAA biosynthesis depend on host and disease context.

Limitations of the study

Several important questions remain. Although our genetic and pharmacological studies support a causal contribution of gut microbial BCAA biosynthesis to impaired insulin sensitivity in the experimental mouse models examined, its contribution to human IR and T2DM remains to be established experimentally. In addition, further optimization and characterization of DHAD inhibitors will be required, including potency across microbial DHAD orthologs, selectivity against potential host targets, intestinal and systemic exposure, pharmacokinetic properties, and long-term tolerability and safety. Although 16S rRNA gene sequencing revealed no broad changes in microbial diversity or community structure following 14 days of Compound 1 treatment, potential effects on specific taxa, microbial functions, and other microbiota-derived metabolites remain to be defined. Future studies should determine how microbial BCAA biosynthesis interacts with diet, host metabolism, and disease etiology and whether microbial BCAA pathway activity can identify individuals most likely to respond to pathway-targeted intervention.

RESOURCE AVAILABILITY

Lead contact

Further information and requests for resources and reagents should be directed to and will be fulfilled by the lead contact, Xiaoyu Tang (xtang@microbechembio.org).

Materials availability

Materials generated in this study are available from the lead contact upon reasonable request.

Data availability

The metagenomic and metatranscriptomic data generated in this study are available in the National Center for Biotechnology Information (NCBI) BioProject database under accession number PRJNA1220304. Publicly available sequencing data analyzed in this study were obtained from the NCBI Sequence Read Archive (accession numbers PRJNA422434, PRJNA373901, PRJNA420817, PRJNA615842, PRJNA530971, PRJNA791492), the European Nucleotide Archive (ENA; accession numbers PRJEB12123, PRJEB21528, PRJEB12357, PRJEB14215), the Metagenomics of the Human Intestinal Tract (MetaHIT) consortium (https://www.gutmicrobiotaforhealth.com/metahit/), and the NIH Human Microbiome Project (HMP; http://www.hmpdacc.org). Metabolomic data generated in this study are

Langtaosha (LTS) Preprint doi: https://doi.org/10.65215/LTSpreprints.2026.11.27.000404. This version posted November 27, 2026. The copyright holder for this preprint (which was not certified by peer review) is the author/funder. Creative Commons license: CC Attribution-NonCommercial-NoDerivatives 4.0 https://creativecommons.org/licenses/by-nc-nd/4.0

accessible via the RIKEN DROP Met database (http://prime.psc.riken.jp/menta.cgi/prime/drop_index) under dataset identifier DM0037. The reference human gut microbiome dataset used in this study is available in the European Nucleotide Archive (ENA) under accession number ERP116715.

Code availability

All custom code used for the analyses in this study is publicly available on GitHub at https://github.com/ytcaimingwei/T2DM_gut_microbiota_BCAA.

ACKNOWLEDGMENTS

This work was supported by the Shenzhen Medical Research Fund (B2602043 to X.T., M.C., and F.L.; B2502007 to X.T.), the Major Program of Shenzhen Bay Laboratory (C1012523006 to X.T.), the National Natural Science Foundation of China (32472350 to C.Y.), and Shenzhen Bay Laboratory Startup Funds (21230051 to X.T.). We thank the Shenzhen Bay Laboratory Supercomputing Center for providing computational resources for meta-omics analyses and the Shenzhen Bay Laboratory Mass Spectrometry Platform for technical support.

AUTHOR CONTRIBUTIONS

X.T. and M.C. conceived the study and designed the experimental framework. M.C. performed the meta-omics analyses. F.L., P.W., M.C., and M.Q. collected and provided human fecal samples. M.C., Z.H., and M.Q. performed genome editing of bacterial strains. M.C., M.Q., M.L., C.Y., and T.Y. performed the mouse experiments. J.H., J.Z., and M.Q. performed homology modeling and molecular docking analyses, and J.Z. provided intellectual input into the discovery of gut microbial DHAD inhibitors. M.L., M.C., and Y.C. performed LC-MS-based metabolite quantification. Y.H., B.H., and Y.Y. provided the chemical compounds used in this study. M.S., M.C., and Q.M. performed SPR analyses. M.C. and M.Q. performed additional experiments, including SEM imaging, bacterial growth assays, RT-qPCR, cytokine profiling, and human sample processing. C.Y., M.Q., M.C., and X.Z. performed western blotting. M.C. and X.T. wrote the original draft of the manuscript. X.T. supervised this study. All authors reviewed and edited the manuscript and approved the final version.

DECLARATION OF INTERESTS

The authors declare no competing interests.

Langtaosha (LTS) Preprint doi: https://doi.org/10.65215/LTSpreprints.2026.11.27.000404. This version posted November 27, 2026. The copyright holder for this preprint (which was not certified by peer review) is the author/funder. Creative Commons license: CC Attribution-NonCommercial-NoDerivatives 4.0 https://creativecommons.org/licenses/by-nc-nd/4.0

STAR★METHODS

KEY RESOURCES TABLE

REAGENT or RESOURCE	SOURCE	IDENTIFIER
Antibodies		
Anti beta Actin antibody [AC-15]	ABclonal, Shanghai, China	Cat# AB6276-1002
Anti-α-Actin-1	Sigma-Aldrich	Cat# mab1501
Akt (pan) (C67E7) Rabbit mAb	Cell Signaling Technology (CST)	Cat# 4691
Phospho-Akt (Ser473) (D9E) XP® Rabbit mAb	Cell Signaling Technology (CST)	Cat# 4060T
Multi-rAb™ HRP-Goat Anti-Rabbit Recombinant Secondary Antibody (H+L)	Proteintech	Cat# RGARO01
Multi-rAb™ HRP-Goat Anti-Mouse Recombinant Secondary Antibody (H+L)	Proteintech	Cat# RGAM001
CST 3024T Phospho-IGF-I Receptor beta(Tyr1135/1136)/Insulin Receptor beta(Tyr1150/1151)(19H7) Rabbit mAb	Cell Signaling Technology (CST)	Cat# 3024T
Insulin Receptor beta (E9L5V) XP ® Rabbit mAb	Cell Signaling Technology (CST)	Cat# 23413T
Phospho-AS160 (Thr642) (D27E6) Rabbit mAb	Cell Signaling Technology (CST)	Cat# 8881T
AS160 (C69A7) Rabbit mAb	Cell Signaling Technology (CST)	Cat# 2670T

Langtaosha (LTS) Preprint doi: https://doi.org/10.65215/LTSpreprints.2026.11.27.000404. This version posted November 27, 2026. The copyright holder for this preprint (which was not certified by peer review) is the author/funder. Creative Commons license: CC Attribution-NonCommercial-NoDerivatives 4.0 https://creativecommons.org/licenses/by-nc-nd/4.0

Bacterial and virus strains		
Bacteroides uniformis	Leibniz Institute DSMZ	DSM6597
Bacteroides uniformis Δ*ilvD*	This study	N/A
Phocaeicola vulgatus	ATCC	ATCC 8482
Phocaeicola vulgatus Δ*ilvD*	This study	N/A
Escherichia coli s17-1 λ pir	ATCC	ATCC BAA-2428
Escherichia coli BL21	TransGen Biotech	Cat# CD701-03
Chemicals, peptides, and recombinant proteins		
Brain Heart Infusion Broth	OXOID	Cat# CM1135B
L-Cysteine hydrochloride anhydrous (H-Cys-OH·HCl)	Solarbio Life Sciences	Cat# C0014
Hemin chloride (0.001g)	Qingdao Hope Bio-Technology Co., Ltd., China	Cat# HB0310a
Vitamin K1 (2mg)	Qingdao Hope Bio-Technology Co., Ltd., China	Cat# HB0310b
Sodium salt of daunomycin	Sigma-Aldrich	Cat# 199303
Agar Powder	Solarbio Life Sciences	Cat# A8190
Glycerol	Macklin	Cat# G810575
(3R,4S,5S,6R,7R,9R,11R,12R,13S,14R)-6-(((2S,3R,4S,6R)-4-(Dimethylamino)-3-hydroxy-6-methyltetrahydro-2H-pyran-2-yl)oxy)-14-ethyl-7,12,13-trihydroxy-4-(((2R,4R,5S,6S)-5-hydroxy-4-methoxy-4,6-dimethyltetrahydro-2H-pyran-2-yl)oxy)-3,5,7,9,11,13-hexamethyloxacyclotetradecane-2,10-dione, Erythromycin	Bidepharm	Cat# BD17733

Langtaosha (LTS) Preprint doi: https://doi.org/10.65215/LTSpreprints.2026.11.27.000404. This version posted November 27, 2026. The copyright holder for this preprint (which was not certified by peer review) is the author/funder. Creative Commons license: CC Attribution-NonCommercial-NoDerivatives 4.0 https://creativecommons.org/licenses/by-nc-nd/4.0

Chloramphenicol	BBI (Shanghai Biotech Co., Ltd.)	Cat# A800118-0050
Ampicillin sodium	BBI (Shanghai Biotech Co., Ltd.)	Cat# A610028-0025
Kanamycin sulfate	aladdin	Cat# K103024-25g
Anhydrotetracycline	Takara Bio Inc.	Cat# 631310
Methanol	Energy Chemical	Cat# A040901
Acetonitrile	J&K Science	Cat# 168171
Ethanol	MREDA Technology Inc.	Cat# M161-4
PBS pH 7.4 basic (1X)	Gibco	Cat# C10010500BT
PrimeSTAR® Max DNA Polymerase	Takara Bio Inc.	Cat# R045A
2 × Phanta Max Master Mix (Dye Plus)	Vazyme	Cat# P525-02
Human insulin	HARVEYBIO	Cat# 11061-68-0
NEBuilder HiFi DNA Assembly Master Mix	NEW ENGLAND Biolabs	Cat# E2621L
Imidazole Propionate	KKL Med	Cat# KCM10234
Leucine	HARVEYBIO	Cat# 61-90-5
Isoleucine	HARVEYBIO	Cat# 73-32-5
Valine	HARVEYBIO	Cat# 72-18-4
Glycine	Shanghai Aladdin Biochemical Technology Co., Ltd.	CAS: 56-40-6
1M Tris-HCl Buffer	Coolaber Science & Technology	Cat# SL3080
PMSF	Bidepharm	Cat# 329-98-6
NP-40 Lysis Buffer	Beyotime Biotechnology	Cat# P0013F
Sodium deoxycholate	SIGMA-ALDRICH Co.	Cat# D6750

Langtaosha (LTS) Preprint doi: https://doi.org/10.65215/LTSpreprints.2026.11.27.000404. This version posted November 27, 2026. The copyright holder for this preprint (which was not certified by peer review) is the author/funder. Creative Commons license: CC Attribution-NonCommercial-NoDerivatives 4.0 https://creativecommons.org/licenses/by-nc-nd/4.0

Sodium orthovanadate Solution	Coolaber Science & Technology	Cat# SL1082
Sodium fluoride	Meryer	CAS: 7681-49-4
β-Glycerol phosphate disodium salt hydrate	MREDA	Cat# M048077
Protease Inhibitor Cocktail (EDTA-free, 100X in DMSO) 100x	Bidepharm	Cat# BD01228199
BSA	HARVEYBIO	Cat# 9048-46-8
1×TBST, PH7.5	MREDA	Cat# M052491
Skim Milk	HARVEYBIO	Cat# SR1764
Tris	BBI (Shanghai Biotech Co., Ltd.)	Cat# A610195
SimplePAGE Plus 4~20% Bis-Tris SDS-PAGE Gel,12wells	BBI (Shanghai Biotech Co., Ltd.)	Cat# C691304-0001
Immobilon® -P PVDF Membrane	Millipore	Cat# IPVH00010
BeyoECL Star	Beyotime Biotechnology	Cat# P0018AS
Multicolor Prestained Protein Ladder	Shanghai Epizyme Biomedical Technology Co., Ltd	Cat# WJ103
2,3-Dihydroxy-3-methylpentanoic acid	Bidepharm	Cat# 562-43-6
3-Methyl-2-oxovaleric acid	MedChemExpress	Cat# HY-113063R
TPEN	GLPBIO	Cat # TPEN
2,4-Dinitrophenylhydrazine	Macklin	Cat# 119-26-6
dithiothreitol	Aladdin	Cat# 1,4-Dithiothreitol (DTT)
2,4-Dinitrophenylhydrazine (DNPH)	Macklin	Cat# D824170
Aspterric acid	Adipogen	Cat# AG-CN2-0132-M001
Pyruvic acid	Yuanye Bio	Cat# S30955
L-Threonine	Aladdin	Cat# T108221
M9 culture medium	Coolaber	Cat# SL00603
DMSO	Merck	Cat# D2650
α-hydroxycarboxylic acid analogs	He et al.[31]	N/A

Langtaosha (LTS) Preprint doi: https://doi.org/10.65215/LTSpreprints.2026.11.27.000404. This version posted November 27, 2026. The copyright holder for this preprint (which was not certified by peer review) is the author/funder. Creative Commons license: CC Attribution-NonCommercial-NoDerivatives 4.0 https://creativecommons.org/licenses/by-nc-nd/4.0

Critical commercial assays		
E.Z.N.A.® Plasmid Mini Kit I	Omega Bio-Tek, Inc.	Cat# D6943-02
E.Z.N.A.® Gel Extraction Kit	Omega Bio-Tek, Inc.	Cat# D2500-02
Takara MiniBEST Bacterial Genomic DNA Extraction Kit Ver.3.0	Takara Bio Inc.	Cat# 9763
FastDNA™ SPIN Kit for Soil	MP Biomedicals	Cat# 6560200
Mouse IL-6 ELISA KIT	Yi Fei Xue Bio Technology	Cat# YFXEM00045
Mouse TNF-α ELISA KIT	Yi Fei Xue Bio Technology	Cat# YFXEM00031
Mouse Resistin ELISA KIT	Yi Fei Xue Bio Technology	Cat# YFXEM00471
Mouse IL-1β ELISA KIT	Yi Fei Xue Bio Technology	Cat# YFXEM00028
Mouse MCP-1 ELISA KIT	Yi Fei Xue Bio Technology	Cat# YFXEM00620
BCA Protein Assay Kit	GLPBIO	Cat# GK10009
Pro Taq HS Premix Probe qPCR Kit	Accurate Biology	Cat# AG11704
Deposited data		
Metagenome and metatranscriptome	This study	PRJNA1220304
Metagenome datasets	NCBI	PRJNA422434
		PRJNA373901
		PRJNA420817
		PRJNA615842
		PRJNA530971
		PRJNA791492
Metagenome datasets	European Nucleotide Archive	PRJEB12123
		PRJEB21528
		PRJEB12357
		PRJEB14215

Langtaosha (LTS) Preprint doi: https://doi.org/10.65215/LTSpreprints.2026.11.27.000404. This version posted November 27, 2026. The copyright holder for this preprint (which was not certified by peer review) is the author/funder. Creative Commons license: CC Attribution-NonCommercial-NoDerivatives 4.0 https://creativecommons.org/licenses/by-nc-nd/4.0

Metagenome datasets	MetaHIT consortium	https://www.gutmicrobiotaforhealth.com/metahit/
Metagenome datasets	Human Microbiome Project	http://www.hmpdacc.org
Metabolome	RIKEN DROP Met database	DM0037
Reference human gut microbiome	European Nucleotide Archive	ERP116715
Metagenome and metatranscriptome	This study	PRJNA1220304
Metagenome datasets	NCBI	PRJNA422434
Experimental models: Organisms/strains		
C57BL/6J male mice (5-6 weeks)	Beijing Vital River Experimental Animal Company	N/A
C57BL/6J male mice (GF, 7-8 weeks)	Shenzhen Gnotobio Biotechnology Co., Ltd.	N/A
C57BL/6J male mice (16 weeks, normal diet)	Beijing Vital River Experimental Animal Company	N/A
C57BL/6J male mice (18 weeks, DIO model induced by high-fat diet starting at 6 weeks old)	Beijing Vital River Experimental Animal Company	N/A
db/db male mice (C57BLKS/J, 7-8 weeks)	GemPharmatech	N/A
m/m male mice (WT, C57BLKS/J, 7-8 weeks)	GemPharmatech	N/A
Experimental models: Cell lines		
Caco-2 human colorectal adenocarcinoma cell line	ATCC	Caco-2
HepG2 human hepatocellular carcinoma cell line	ATCC	HepG2
HEK-293 human embryonic kidney cell line	ATCC	HEK-293

Langtaosha (LTS) Preprint doi: https://doi.org/10.65215/LTSpreprints.2026.11.27.000404. This version posted November 27, 2026. The copyright holder for this preprint (which was not certified by peer review) is the author/funder. Creative Commons license: CC Attribution-NonCommercial-NoDerivatives 4.0 https://creativecommons.org/licenses/by-nc-nd/4.0

Oligonucleotides		
See Table S6 for primers for amplicon and RT-qPCR	This study	N/A
CGGGCTTAAATTGCAGATGA	Tong et al.[37]	Pv-TaqMan-F
CATGCAGCACCTTCACAGAT	Tong et al.[37]	Pv-TaqMan-R
TGAAAGCCGTAAGCCGCAAGG	Tong et al.[37]	Pv-probe
TCTTCCGCATGGTAGAACTATTA	Tong et al.[37]	Bu-TaqMan-F
ACCGTGTCTCAGTTCCAATGTG	Tong et al.[37]	Bu-TaqMan-R
CGTTCCATTAGGTTGTTGGCGGGG	Tong et al.[37]	Bu-probe
Recombinant DNA		
pB025	Zheng et al.[38]	N/A
Software and algorithms		
MetaWRAP (v1.3.2)	Uritskiy et al.[39]	https://github.com/bxlab/metaWRAP
GTDB-Tk (v2.1.1)	Chaumeil et al.[40]	https://github.com/Ecogenomics/GTDBTk
dRep (v3.4.3)	Olm et al.[41]	https://github.com/MrOlm/drep
CheckM (v1.2.2)	Parks et al.[42]	
IQ-TREE (v2.2.2.7)	Minh et al.[43]	https://iqtree.github.io/
iTOL	Letunic and Bork[44]	https://itol.embl.de/
Salmon (v0.13.1)	Patro et al.[45]	https://github.com/COMBINE-lab/salmon
pyani (v0.2.8)	Pritchard et al.[46]	https://github.com/widdowquinn/pyani
CompareM (v0.1.2)	N/A	https://github.com/dparks1134/CompareM
Prodigal (v2.6.3)	N/A	https://github.com/hyattpd/prodigal
eggNOG-mapper (v2.1.7)	Huerta-Cepas et al.[47]	https://github.com/eggnogdb/eggnog-mapper
Sickle (v1.33)	Joshi et al.[48]	https://github.com/najoshi/sickle
BBMap (v35.x)	Bushnell[49]	https://github.com/BioInfoTools/BBMap
CoverM (v0.6.1)	N/A	https://github.com/wwood/CoverM
R project (v4.2.1)	N/A	https://www.r-project.org/
edgeR (v4.2.1) in R project	N/A	https://bioc.r-universe.dev/edgeR

Langtaosha (LTS) Preprint doi: https://doi.org/10.65215/LTSpreprints.2026.11.27.000404. This version posted November 27, 2026. The copyright holder for this preprint (which was not certified by peer review) is the author/funder. Creative Commons license: CC Attribution-NonCommercial-NoDerivatives 4.0 https://creativecommons.org/licenses/by-nc-nd/4.0

Caret in R project	N/A	https://topepo.github.io/caret/index.html
randomForest in R project	N/A	https://cran.r-project.org/web/packages/randomForest/index.html
SIAMCAT in R project	N/A	https://siamcat.embl.de/
SnapGene (v6.0.2)	N/A	https://www.snapgene.com/
ImageJ	N/A	https://imagej.net/ij/
PyMOL (v2.6.0a0)	N/A	https://pymol.org/
AutoDock Vina (v1.5.7)	N/A	https://vina.scripps.edu/
ChemDraw (v23.1.1)	N/A	https://revvitysignals.com/products/research/chemdraw
Other		

METHOD DETAILS

In-house cohort for multi-omics analysis and sample processing

Fecal samples were collected from five participants with T2DM and four healthy controls in Shenzhen, China. Individuals with severe gastrointestinal diseases, including gastrointestinal malignancy or inflammatory bowel disease, or major T2DM-associated complications, such as coronary artery disease, were excluded. Fresh fecal samples were transported under temperature-controlled conditions, processed within 24 h of collection, and subjected to parallel extraction of genomic DNA and total RNA for subsequent multi-omics analyses. The study was approved by the Ethics Committee of Shenzhen University of Advanced Technology General Hospital, formerly Shenzhen Hospital of the University of Chinese Academy of Sciences (approval No. LL-KT-2020147).

Genomic DNA was extracted using the ALFA-SEQ Advanced Stool DNA Kit (Magenbio, Guangzhou, China), and total RNA was extracted using the HiPure Universal RNA Mini Kit (Magenbio), according to the manufacturers' instructions. Metagenomic DNA libraries were prepared using the ALFA-SEQ DNA Library Prep Kit (Magenbio). Metatranscriptomic messenger RNA libraries were prepared using the NEBNext® Ultra™ Nondirectional RNA Library Prep Kit for Illumina® (New England Biolabs, Ipswich, MA, USA). All libraries were subjected to 150-bp paired-end sequencing on an Illumina NovaSeq 6000 platform (Illumina, San Diego, CA, USA).

Reconstruction of MAGs

In-house shotgun metagenomic sequencing data were integrated with data from five

Langtaosha (LTS) Preprint doi: https://doi.org/10.65215/LTSpreprints.2026.11.27.000404. This version posted November 27, 2026. The copyright holder for this preprint (which was not certified by peer review) is the author/funder. Creative Commons license: CC Attribution-NonCommercial-NoDerivatives 4.0 https://creativecommons.org/licenses/by-nc-nd/4.0

previously published cohorts, including the HMP,[25] Jie et al.,[26] Karlsson et al.,[27] MetaHIT,[28] and Qin et al.[29]. Metagenomic data were processed using the metaWRAP pipeline (v1.3.2)[39] following standard operating procedures. Briefly, raw sequencing reads underwent a two-step quality-control procedure using the metaWRAP Read_qc module. Adapter sequences and low-quality reads were first removed, followed by removal of reads mapping to the human reference genome to minimize host DNA contamination. The remaining high-quality reads were assembled *de novo* into contigs using metaSPAdes through the metaWRAP Assembly module. The assembled contigs were independently binned using MetaBAT2, MaxBin2, and CONCOCT with default parameters. The resulting draft bins were subsequently refined and reassembled using the parameters "-c 50 -x 10," generating medium-quality MAGs with >50% completeness and <10% contamination, in accordance with the Minimum Information about a Metagenome-Assembled Genome (MIMAG) standards.[50] Ribosomal RNA genes were identified in the reconstructed MAGs using Barrnap (v0.9). The relative abundance of each MAG across samples was estimated using the metaWRAP Quant_bins module, with abundance values normalized and expressed as transcripts per million (TPM), for subsequent comparative genomic and statistical analyses.

Genomic characterization and phylogenetic reconstruction of MAGs

Taxonomic classification of qualified MAGs was performed using the Genome Taxonomy Database Toolkit (GTDB-Tk, v2.1.1)[40] against the Genome Taxonomy Database (GTDB, release 207). Species-level dereplication was conducted using dRep (v3.4.3)[41] with a species demarcation threshold of 95% average nucleotide identity (ANI) and a minimum genome alignment coverage of 50%.[51] This analysis yielded 2,894 non-redundant, species-representative MAGs.

Universal single-copy bacterial marker genes were identified using CheckM (v1.2.2).[42] The marker genes were aligned, and a maximum-likelihood phylogenetic tree was constructed using IQ-TREE (v2.2.2.7).[43] Substitution models were selected automatically, and branch support was evaluated using 1,000 ultrafast bootstrap replicates. Phylogenetic trees and associated taxonomic and functional annotations were visualized and edited using the Interactive Tree of Life platform (iTOL, https://itol.embl.de/).[44]

Identification of T2DM-associated gut microbiota using integrated statistical and machine learning approaches

An integrated statistical and machine-learning workflow was used to identify microbial signatures associated with T2DM. Differential abundance analysis was performed using the edgeR package (v4.2.1) in R, based on the Salmon-derived read count generated by

Langtaosha (LTS) Preprint doi: https://doi.org/10.65215/LTSpreprints.2026.11.27.000404. This version posted November 27, 2026. The copyright holder for this preprint (which was not certified by peer review) is the author/funder. Creative Commons license: CC Attribution-NonCommercial-NoDerivatives 4.0 https://creativecommons.org/licenses/by-nc-nd/4.0

the metaWRAP Quant_bins module. Microbial features were considered differentially abundant according to the predefined thresholds described in the corresponding analyses, including a $|\log_2$ fold change$| \geq 1$ and false discovery rate (FDR)-adjusted $p < 0.05$.[52,53]

Support vector machine (SVM) and random forest (RF) classifiers were applied to identify complementary microbial signatures associated with T2DM. The dataset was divided into training and held-out testing subsets at an 80:20 ratio using stratified random sampling implemented with the caret package. The RF classifier was trained using the randomForest package, whereas a linear-kernel SVM classifier was trained using the e1071 package. Feature scaling for the SVM was performed using parameters estimated exclusively from the training data. Model performance was evaluated using receiver operating characteristic (ROC) curve analysis and area under the ROC curve (AUC) on the independent held-out testing subset. In addition, stratified 10-fold cross-validation was performed within the training set to estimate cross-validated AUC values. Feature prioritization was based on model-derived importance measures, including mean decrease in Gini impurity for RF and the absolute coefficients of the linear SVM. Microbial taxa with established or plausible functional associations with host metabolic regulation were subsequently considered for biological interpretation. All analyses were performed in R (v4.2.1).

Functional profiling of microbial enzymes in IR-associated metabolic pathways

Integrated metagenomic and metatranscriptomic analyses were performed to characterize microbial enzymes involved in amino acid metabolic pathways associated with insulin resistance (IR). Protein-coding genes were predicted using Prodigal (v2.6.3) and functionally annotated with eggNOG-mapper (v2.1.7), as well as against the customized dbCAN and TCDB databases. Genes associated with amino acid metabolism were selected for downstream analysis (Table S4). Gene abundance in the metagenomic datasets and transcript abundance in the metatranscriptomic datasets were quantified using Salmon (v0.13.1) with default parameters.[45]

Selection and preparation of bacterial strains for functional validation

A phylogenetically guided strategy was used to select representative bacterial strains for *in vitro* and *in vivo* functional validation. Reference genomes from GTDB, newly reconstructed MAGs, and experimentally validated type-strain genomes were combined to construct a maximum-likelihood phylogenetic tree using IQ-TREE (v2.2.2.7). The tree was visualized using iTOL.

Genomic similarity was assessed using ANI and average amino acid identity (AAI). ANI was calculated using pyani (v0.2.8),[46] and AAI was calculated using CompareM

Langtaosha (LTS) Preprint doi: https://doi.org/10.65215/LTSpreprints.2026.11.27.000404. This version posted November 27, 2026. The copyright holder for this preprint (which was not certified by peer review) is the author/funder. Creative Commons license: CC Attribution-NonCommercial-NoDerivatives 4.0 https://creativecommons.org/licenses/by-nc-nd/4.0

(v0.1.2; https://github.com/dparks1134/CompareM) with default parameters.

Based on the combined phylogenetic and genomic similarity analyses, *B. uniformis* DSM 6597 and *P. vulgatus* ATCC 8482 were obtained from the Bena Culture Collection (Beijing, China). These strains were selected because of their high genomic similarity to the T2DM-associated MAGs identified in the clinical cohort. *B. uniformis* DSM 6597 showed 84.6% AAI and 98.2% ANI to its matched clinical MAG, whereas *P. vulgatus* ATCC 8482 showed 78.4% AAI and 98.4% ANI to its corresponding MAG (Figure S4).

The bacterial strains were revived on Columbia blood agar plates and routinely cultured in Brain Heart Infusion (BHI) medium supplemented with 5 μg/mL hemin chloride and 10 μg/mL vitamin K1. Cultures were maintained at 37°C under strictly anaerobic conditions. For oral gavage, bacterial suspensions were prepared in pre-reduced anaerobic BHI medium and standardized to the required concentration. Bacterial viability was confirmed by serial dilution and colony counting on BHI agar plates before each gavage procedure. All bacterial manipulations were performed in an anaerobic workstation.

Genetic engineering of bacterial strains

A previously established pB025 plasmid system was used for targeted *ilvD* gene deletion in human gut Bacteroides species.[38] The pB025 backbone was linearized by inverse PCR, and the flanking homology arms (~500 bp each) were separately amplified from genomic DNA of the target strain. All primer pairs are listed in Table S6 and were designed using SnapGene (v6.0.2). PCR products were purified, and their concentrations were determined prior to assembly.

The knockout construct was assembled using the NEBuilder HiFi DNA Assembly Master Mix (New England Biolabs). The assembly reaction contained the linearized pB025 vector backbone, the upstream homology arm, and the downstream homology arm at an optimized molar ratio (vector:upstream:downstream = 1:3:3). The two homology arms were designed to flank the *ilvD* coding sequence—positioned upstream and downstream of the target gene, respectively—to enable precise deletion of the coding region via homologous recombination. The assembled plasmids were subjected to Sanger sequencing across all ligation junctions (Sangon Biotech, Guangzhou, China) to confirm construct integrity before transfer into recipient bacterial strains.

Conjugation-mediated plasmid transfer and generation of *ilvD* knockout mutants

The sequence-verified pB025 knockout plasmid was introduced into recipient strains via intergeneric conjugation.[54] Prior to conjugation, the knockout plasmid was electroporated into *E. coli* S17-1 donor cells using a single 2,500-V pulse (Eppendorf Eporator). Transformants were selected on LB agar containing 25 μg/mL ampicillin.

Langtaosha (LTS) Preprint doi: https://doi.org/10.65215/LTSpreprints.2026.11.27.000404. This version posted November 27, 2026. The copyright holder for this preprint (which was not certified by peer review) is the author/funder. Creative Commons license: CC Attribution-NonCommercial-NoDerivatives 4.0 https://creativecommons.org/licenses/by-nc-nd/4.0

Recipient strains (*B. uniformis* DSM 6597 and *P. vulgatus* ATCC 8482) were pre-cultured anaerobically to mid-logarithmic phase (OD_{600} = 0.2–0.3, corresponding to ~10^8 CFU/mL, measured after vigorous vortexing). Donor and recipient cells were mixed at a 1:1 ratio (based on OD_{600}), pelleted, resuspended, and evenly spread onto non-selective BHI agar plates supplemented with 20 mM $MgCl_2$ (to enhance conjugation efficiency). After 24 h of anaerobic incubation at 37 °C, the entire bacterial lawn was scraped, resuspended in 1 mL of PBS, and serially diluted (10^{-1} to 10^{-5}). Aliquots were plated onto pre-reduced BHI blood agar supplemented with 50 μg/mL gentamicin (to counterselect the *E. coli* donor) and 25 μg/mL erythromycin (to select for pB025-containing transconjugants). Putative transconjugants were validated by colony PCR and Sanger sequencing across the *ilvD* junction regions to confirm the presence of the knockout construct.

For the excision of the selection cassette, three verified transconjugants per strain were inoculated into 8 mL of pre-reduced BHI broth without erythromycin but containing 200 ng/mL anhydrotetracycline (aTc) to induce Cas12a-mediated excision of the selection cassette. After 24 h of induction, cultures were diluted and plated onto pre-reduced BHI agar containing 200 ng/mL aTc (without erythromycin). Individual colonies were replica-plated onto BHI agar with and without 25 μg/mL erythromycin to screen for erythromycin sensitivity. Clones that failed to grow on erythromycin-containing plates were selected as candidates for marker loss. Loss of the *ilvD* coding region was confirmed by colony PCR and Sanger sequencing.

For plasmid curing, each strain was serially passaged five times in antibiotic-free, pre-reduced BHI medium with a 1:100 dilution at each passage. This approach was chosen based on our preliminary observation that five passages were sufficient to eliminate the plasmid from the majority of cells, as judged by replica-plating. After the final passage, cultures were diluted and plated onto non-selective BHI agar. Individual colonies were screened for the loss of plasmid-encoded erythromycin resistance via replica-plating on BHI agar with and without 25 μg/mL erythromycin. Clones exhibiting an erythromycin-sensitive phenotype were selected, and the absence of the pB025 backbone was further confirmed by PCR using primers targeting the *repB* gene. The final plasmid-free, marker-free knockout strains were designated *B. uniformis* Δ*ilvD* (*Bu* Δ*ilvD*) and *P. vulgatus* Δ*ilvD* (*Pv* Δ*ilvD*).

Bacterial growth kinetics

The *in vitro* growth kinetics of wild-type and mutant strains, including *Bu* WT, *Bu* Δ*ilvD*, *Pv* WT, and *Pv* Δ*ilvD*, were evaluated under standardized anaerobic conditions. Each strain was first cultured overnight in pre-reduced BHI medium at 37°C. Overnight cultures were diluted to an identical starting OD_{600} of 0.05 and inoculated into fresh pre-reduced BHI

Langtaosha (LTS) Preprint doi: https://doi.org/10.65215/LTSpreprints.2026.11.27.000404. This version posted November 27, 2026. The copyright holder for this preprint (which was not certified by peer review) is the author/funder. Creative Commons license: CC Attribution-NonCommercial-NoDerivatives 4.0 https://creativecommons.org/licenses/by-nc-nd/4.0

medium. Bacterial growth was monitored at 2-h intervals for 24 h by measuring OD_{600} using an Eppendorf BioPhotometer D30. Three biological replicates were performed for each strain.

Scanning electron microscopy

The cellular morphology of wild-type and Δ*ilvD* mutant strains was examined by scanning electron microscopy. Bacterial suspensions were placed onto aluminum stubs coated with conductive adhesive and fixed with 2.5% glutaraldehyde for 2 h at room temperature. Samples were washed thoroughly with 0.1 M phosphate-buffered saline (PBS; pH 7.4) and post-fixed for 1 h in a mixture of 1% osmium tetroxide and 0.15% potassium ferrocyanide.

Samples were dehydrated through a graded ethanol series from 30% to 100%, with a 10-min incubation at each concentration, and subsequently subjected to critical-point drying. Dried samples were sputter-coated with a 10-nm layer of gold–palladium. Images were acquired using a Gemini 360 scanning electron microscope (Zeiss) under high-vacuum conditions at an accelerating voltage of 5 kV and a working distance of 5 mm.

***In vivo* assessment of bacterial strains in mouse models**

All animal procedures were approved by the Institutional Animal Care and Use Committee of Shenzhen Bay Laboratory (approval No. AETXY202302) and conducted in accordance with the Guide for the Care and Use of Laboratory Animals.

Male C57BL/6J mice aged 5–6 weeks and weighing 20–25 g were obtained from Beijing Vital River Experimental Animal Company. Mice were housed in a specific-pathogen-free (SPF) facility under a 12-h light/dark cycle at an ambient temperature of 25 ± 1°C and relative humidity of 60% ± 5%. Animals had ad libitum access to autoclaved water and a normal chow diet (NCD; CAS No. 1010088), except when specified dietary interventions were applied.

For dietary intervention experiments, mice were randomly assigned after acclimatization to one of three dietary groups (n = 8 per group): NCD, inulin-enriched diet (IED), or high-fat diet (HFD). All diets were obtained from Jiangsu Xietong Pharmaceutical Bio-engineering Co., Ltd. The IED contained 17.2% protein, 69.4% carbohydrate, and 5.9% fat by weight. The HFD provided 20% of calories from protein, 60% from fat, and 20% from carbohydrate. Dietary interventions began at the initiation of bacterial colonization and continued for 14 days. Food and water were provided *ad libitum*.

For microbiota depletion experiments, mice received a broad-spectrum antibiotic cocktail in their drinking water.[55] The cocktail contained 100 μg/mL neomycin, 50 μg/mL streptomycin, 100 μg/mL ampicillin, 50 μg/mL vancomycin, 100 μg/mL metronidazole, 100 μg/mL bacitracin, 125 μg/mL ciprofloxacin, and 100 μg/mL ceftazidime. Antibiotic solutions

Langtaosha (LTS) Preprint doi: https://doi.org/10.65215/LTSpreprints.2026.11.27.000404. This version posted November 27, 2026. The copyright holder for this preprint (which was not certified by peer review) is the author/funder. Creative Commons license: CC Attribution-NonCommercial-NoDerivatives 4.0 https://creativecommons.org/licenses/by-nc-nd/4.0

were freshly prepared every 24 h and administered continuously for 14 days. Germ-free C57BL/6J mice were obtained from Shenzhen Gnotobio Biotechnology Co., Ltd. and maintained under strict isolator conditions.

For bacterial intervention experiments, mice were randomly allocated to treatment groups with 8 mice per group, received daily oral gavage of 250 μL bacterial suspension (5×10^8 CFU per mouse) containing either wild-type or Δ*ilvD* strains of *B. uniformis* or *P. vulgatus*. Bacterial administration continued for 14 consecutive days. Glucose and insulin tolerance tests were performed under standardized environmental conditions and at consistent times of day. Blood glucose concentrations were measured using a handheld glucometer.

Glucose and insulin tolerance test

Oral glucose tolerance test (OGTT) and insulin tolerance test (ITT) were performed at consistent times of day to minimize circadian variation in glucose homeostasis.

For OGTT, mice were fasted overnight for 12 h with free access to sterile drinking water. Glucose was administered orally at a dose of 2 g/kg body weight. Blood glucose was measured from tail-vein blood at 0, 15, 30, 60, 90, and 120 min after glucose administration using an Accu-Chek handheld glucometer. For ITT, mice were fasted for 4 h and then injected intraperitoneally with regular insulin at a dose of 1 U/kg body weight. Blood glucose was measured at the same time points used for the OGTT.

BCAA quantification in bacterial cultures and mouse fecal samples

For analysis of BCAA production by 114 human gut bacterial isolates, bacterial cultures were centrifuged at 15,000 × g for 10 min at 4°C to obtain cell-free supernatants. Supernatants were diluted 1:100 with 50% acetonitrile (v/v) to a final acetonitrile concentration of ~50%, followed by centrifugation at 15,000 × *g* for 30 min at 4°C to precipitate residual proteins and remove particulates. Clarified supernatants were analyzed by targeted liquid chromatography–tandem mass spectrometry (LC–MS/MS).

Leucine, isoleucine, and valine were quantified in multiple reaction monitoring (MRM) mode using an Agilent 1290 Infinity II liquid chromatograph coupled to an Agilent 6470 triple quadrupole mass spectrometer equipped with an Agilent Jet Stream (AJS) electrospray ionization source operating in positive ion mode. Chromatographic separation was performed on an XBridge Amide column (3.5 μm, 4.6 × 100 mm). Mobile phase A consisted of 10 mM ammonium formate in water, and mobile phase B consisted of 10 mM ammonium formate in 90% acetonitrile/water (v/v). The gradient was held at 98% B for 15 min, then returned to initial conditions for re-equilibration. The flow rate was 0.5 mL/min, and the injection volume was 2 μL. The column temperature was maintained at 25°C, and

Langtaosha (LTS) Preprint doi: https://doi.org/10.65215/LTSpreprints.2026.11.27.000404. This version posted November 27, 2026. The copyright holder for this preprint (which was not certified by peer review) is the author/funder. Creative Commons license: CC Attribution-NonCommercial-NoDerivatives 4.0 https://creativecommons.org/licenses/by-nc-nd/4.0

the autosampler temperature was set at 4°C.

Mass spectrometric parameters were as follows: gas temperature 300°C, gas flow 10 L/min, nebulizer pressure 45 psi, sheath gas temperature 350°C, sheath gas flow 11 L/min, capillary voltage 3500 V, and nozzle voltage 500 V. The MRM transitions, optimized for each analyte, were: leucine/isoleucine, m/z 132.1 → 86 (fragmentor 80 V, collision energy 8 V, cell accelerator voltage 5 V); valine, m/z 118.1 → 72 (fragmentor 80 V, collision energy 10 V, cell accelerator voltage 5 V). A dwell time of 200 ms was used per transition. Data acquisition and processing were performed using Agilent MassHunter software.

Quantification was performed using external calibration curves prepared in blank culture medium matrix. Calibration standards were prepared at concentrations ranging from 0.625 to 160 mg/L. A fresh calibration curve was run with each batch of samples, and all calibration curves exhibited excellent linearity with $R^2 > 0.999$. BCAA concentrations in bacterial cultures were normalized to bacterial density based on OD600 measurements. Samples were analyzed in three biological replicates.

For fecal BCAA quantification, mouse fecal samples (~20 mg) were homogenized in ice-cold 100% methanol at a ratio of 1:10 (w/v) using a TissueMaster™ handheld homogenizer and sonicated in an ice bath for 2 h. Samples were centrifuged at 15,000 × g for 10 min at 4°C, and the resulting supernatants were transferred to fresh tubes and concentrated to dryness using an Eppendorf Concentrator Plus™. Dried extracts were reconstituted in 50% acetonitrile, centrifuged at 15,000 × *g* for 10 min at 4°C to remove insoluble material, and the clarified supernatants were stored at −80°C until LC-MS/MS analysis. Fecal BCAA concentrations were quantified using the same LC-MS/MS method and calibration curve strategy described above for bacterial culture supernatants.

Quantitative assessment of bacterial colonization in mouse feces

Absolute bacterial colonization levels were quantified using probe-based quantitative real-time PCR (qPCR). Fresh fecal pellets were collected from individual mice at three time points: after a 1-week acclimatization period, immediately after completion of the 14-day antibiotic treatment in antibiotic-treated cohorts, and at the end of the 14-day bacterial gavage period.

Fecal samples were immediately snap-frozen in liquid nitrogen and stored at −80°C until DNA extraction. Total genomic DNA was extracted from weighed fecal pellets using the FastDNA™ SPIN Kit for Soil according to the manufacturer's instructions. DNA concentration and purity were assessed using a NanoDrop spectrophotometer.

qPCR was performed using a QuantStudio™ 6 Pro Real-Time PCR System and the Pro Taq HS Premix Probe qPCR Kit (Accurate Biology, Hunan, China). Each 20-μL reaction contained 1 μL of normalized genomic DNA, 0.4 μL of each target-specific forward and

Langtaosha (LTS) Preprint doi: https://doi.org/10.65215/LTSpreprints.2026.11.27.000404. This version posted November 27, 2026. The copyright holder for this preprint (which was not certified by peer review) is the author/funder. Creative Commons license: CC Attribution-NonCommercial-NoDerivatives 4.0 https://creativecommons.org/licenses/by-nc-nd/4.0

reverse primer, 10 μL of 2× Pro Taq HS Probe Premix, 0.3 μL of the corresponding hydrolysis probe listed in Table S6,[37] 0.4 μL of ROX reference dye, and 7.5 μL of nuclease-free water. The cycling program consisted of an initial denaturation step at 95°C for 2 min, followed by 40 cycles of denaturation at 95°C for 15 s and annealing/extension at 60°C for 15 s. A final extension was performed at 72°C for 30 s.

Western blot analysis of insulin signaling

To assess host insulin signaling, liver, epididymal white adipose tissue (eWAT), and gastrocnemius muscle were collected from germ-free C57BL/6 mice colonized with Bu WT or *Bu* Δ*ilvD*. Tissues were immediately snap-frozen in liquid nitrogen and homogenized in NP-40 lysis buffer containing 50 mM Tris-HCl (pH 7.4), 150 mM NaCl, and 1% NP-40. The buffer was supplemented with 1 mM phenylmethylsulfonyl fluoride, 10 mM β-glycerophosphate, 1 mM sodium orthovanadate, 20 mM sodium fluoride, and EDTA-free protease inhibitor cocktail.

Homogenates were centrifuged at 12,000 × *g* for 15 min at 4°C. Total protein concentrations were determined using a bicinchoninic acid assay. Equal amounts of protein were separated by 4%–20% gradient SDS-PAGE, with 10 μg of protein loaded per lane, and transferred to polyvinylidene fluoride membranes.

Membranes were blocked with 5% bovine serum albumin in TBST and incubated with an antibody against p-Akt (Ser473), total Akt, β-actin and α-actin. After incubation with HRP-conjugated secondary antibodies, protein bands were visualized using enhanced chemiluminescence on a ChemiDoc™ imaging system. β-actin was used as the loading control, and a multicolor prestained protein ladder was used for molecular-weight calibration. Three biological replicates were analyzed for each experimental condition. Band intensities were quantified using ImageJ software. P-Akt signals were normalized to the corresponding total Akt signal for each sample.

Cytokine quantification

Whole blood samples were centrifuged at 2,000 × *g* for 10 min at 4°C to separate serum. Serum samples were aliquoted and stored at −20°C until analysis. Serum concentrations of IL-6, TNF-α, IL-1β, monocyte chemoattractant protein 1 (MCP-1), and resistin were measured using commercial ELISA kits (Yi Fei Xue BioTechnology) according to the manufacturers' instructions.

Protein lysates were prepared from liver, eWAT, and skeletal muscle, and the identical panel of cytokines (IL-6, TNF-α, IL-1β, MCP-1, and resistin) was quantified in each of the three tissues using the same ELISA kits. Standard curves were included on each plate, and all measurements were performed in three technical replicates.

Langtaosha (LTS) Preprint doi: https://doi.org/10.65215/LTSpreprints.2026.11.27.000404. This version posted November 27, 2026. The copyright holder for this preprint (which was not certified by peer review) is the author/funder. Creative Commons license: CC Attribution-NonCommercial-NoDerivatives 4.0 https://creativecommons.org/licenses/by-nc-nd/4.0

Comprehensive profiling and functional annotation of human gut microbiome data

Large-scale phylogenetic and functional profiling was performed using a publicly available human gut microbial genome dataset.[56] The dataset contained 204,938 reference genomes and MAGs. A total of 4,789 non-redundant, species-level representative genomes and MAGs were selected for downstream analysis. The dataset included genomes from geographically diverse human cohorts and was primarily composed of members of the classes Clostridia, Bacteroidia, Gammaproteobacteria, and Bacilli.

All representative genomes and MAGs were uniformly annotated using eggNOG-mapper (v2.1.7) against the eggNOG database (v5.0.2).[47] Metabolic pathway reconstruction focused on IR-associated metabolic processes, with particular emphasis on BCAA biosynthesis and related amino acid metabolic pathways. Functional annotations were assigned using the Kyoto Encyclopedia of Genes and Genomes database,[57] supplemented by manual curation based on published literature.[6,58-69]

Phylogenetic analyses of core BCAA biosynthetic genes were performed using IQ-TREE (v2.2.2.7) with the Q.yeast+I+R10 substitution model and 1,000 ultrafast bootstrap replicates. The phylogenetic tree was visualized using iTOL, with functional metadata mapped to the corresponding tree nodes.

Homology modeling and molecular docking analysis

Three-dimensional structures of *Bu*_DHAD and *Pv*_DHAD were generated by homology modeling using the high-resolution crystal structure of *Arabidopsis thaliana* DHAD-AA (PDB ID: 9JPI) as the template. Molecular docking simulations were performed using AutoDock Vina (v1.5.7) to characterize the binding poses of aspterric acid and Compound 1 within the conserved DHAD catalytic pocket. Structural superposition of DHAD orthologs, visualization of catalytically relevant residues, and preparation of structural figures were performed using PyMOL (v2.6.0a0).

DHAD protein expression and purification

Recombinant DHAD proteins were expressed in *E. coli* BL21 cells harboring the corresponding expression constructs. Cultures were grown in Terrific Broth supplemented with 50 μg/mL kanamycin at 37°C with shaking at 250 rpm until the OD_{600} reached approximately 0.6. Protein expression was induced by adding 0.5 mM isopropyl β-D-1-thiogalactopyranoside. Cultures were incubated overnight at 16°C with shaking at 250 rpm. Cells were harvested by centrifugation at 4,200 rpm for 10 min at 4°C. Cell pellets were resuspended in lysis buffer at a ratio of 5 mL per gram of wet cell mass. The lysis buffer contained 50 mM Tris-HCl, 50 mM NaCl, 10 mM imidazole, 10% glycerol, 1 mM PMSF, and 1 mg/mL lysozyme at pH 8.0. Cell suspensions were incubated on ice for 30 min and

Langtaosha (LTS) Preprint doi: https://doi.org/10.65215/LTSpreprints.2026.11.27.000404. This version posted November 27, 2026. The copyright holder for this preprint (which was not certified by peer review) is the author/funder. Creative Commons license: CC Attribution-NonCommercial-NoDerivatives 4.0 https://creativecommons.org/licenses/by-nc-nd/4.0

lysed by sonication at 200 W using a 3-s on/6-s off pulse cycle for a total sonication time of 30 min.

Lysates were clarified by centrifugation at 20,000 × *g* for 30 min at 4°C, filtered through a 0.45-μm membrane, and loaded onto a 5-mL HisTrap™ HP column (Cytiva) equilibrated with lysis buffer. Bound proteins were eluted using a stepwise imidazole gradient. Elution buffers contained 8%, 25%, 50%, or 100% of 500 mM imidazole in a base buffer consisting of 50 mM Tris-HCl, 500 mM NaCl, and 10% glycerol at pH 8.0. Elution was performed over 5 column volumes at a flow rate of 2 mL/min.

Eluted fractions were analyzed by 4%–20% gradient SDS-PAGE with Coomassie staining. Fractions containing purified DHAD were pooled, concentrated using an Amicon® Ultra-15 centrifugal filter unit with a 30-kDa molecular-weight cutoff, and buffer-exchanged into storage buffer containing 50 mM Tris-HCl, 150 mM NaCl, 5 mM $MgCl_2$, 10% glycerol, and 1 mM DTT at pH 8.0.

The final protein concentration was adjusted to 20 mg/mL and determined by measuring absorbance at 280 nm using an extinction coefficient calculated from the amino acid sequence. Protein aliquots were flash-frozen in liquid nitrogen and stored at −80°C until use.

Characterization of DHAD enzyme activity

DHAD activity was measured in 40-μL reaction mixtures containing 50 mM Tris-HCl (pH 8.5), 1 mM DTT, 10 mM $MgCl_2$, and 1 mM 2,3-dihydroxy-3-methylpentanoic acid (DHMV). Reactions were initiated by adding 10 μM purified DHAD protein and incubated aerobically at 0 °C for 60 min. Reactions were terminated by adding 10 μL of 2 M HCl.

The enzymatically generated 3-methyl-2-oxovaleric acid, also referred to as ketomethylvalerate (KMV), was derivatized *in situ* by adding 20 μL of saturated 2,4-dinitrophenylhydrazine (DNPH) in 2 M HCl. Samples were incubated at room temperature for 60 min. Subsequently, 10 μL of 10 M NaOH was added, and samples were mixed thoroughly. Precipitates were removed by centrifugation at 10,000 × *g* for 10 min.

Quantification was performed using a standard curve generated with the KMV–DNPH adduct. The standard curve was linear over the range of 0–0.5 mM (R^2 = 0.9996). Samples were analyzed by ultra-performance liquid chromatography using an Agilent 1290 Infinity II system equipped with a Kinetex XB-C18 column (2.6 μm, 100 Å, 100 × 4.6 mm). Separation was performed using a 10-min linear gradient from 5% to 95% acetonitrile in 0.1% trifluoroacetic acid at a flow rate of 0.8 mL/min. Quantitative detection was performed by UV absorbance at 380 nm. Heat-inactivated DHAD was prepared by incubation at 60°C for 30 min and used as an enzyme-inactivation control.

Langtaosha (LTS) Preprint doi: https://doi.org/10.65215/LTSpreprints.2026.11.27.000404. This version posted November 27, 2026. The copyright holder for this preprint (which was not certified by peer review) is the author/funder. Creative Commons license: CC Attribution-NonCommercial-NoDerivatives 4.0 https://creativecommons.org/licenses/by-nc-nd/4.0

Screening of DHAD inhibitors

For primary screening, compounds from an in-house library comprising 27 α-hydroxycarboxylic acid analogs and aspterric acid were pre-incubated with *Bu*_DHAD or *Pv*_DHAD at 0°C for 60 min. Enzymatic reactions were initiated by adding DHMV substrate. The complete reaction mixture contained Tris-HCl buffer (pH 8.5), 1 mM DTT, 10 mM $MgCl_2$, 10 μM DHAD protein, 1 mM DHMV, and 100 μM test compound. Reactions were incubated at 37°C for 30 min and terminated by adding one-quarter volume of 2 M HCl. Enzyme activity was quantified as described above.

For dose–response analysis, Compound 1 and Compound 2 were tested at concentrations of 0.1, 1, 10, 100, 500, and 5,000 μM. IC_{50} values were calculated by nonlinear regression of the inhibition curves.

***In vitro* validation of DHAD inhibitors**

The effects of DHAD inhibition on microbial BCAA production were evaluated using *B. uniformis*. Bacteria were pre-cultured anaerobically in BHI medium at 37°C until reaching the mid-exponential phase. Compound 1 was added to bacterial suspensions at final concentrations of 1, 10, or 100 μM. An equivalent volume of DMSO was added to control cultures.

Cultures were incubated anaerobically at 37°C for 2 h. OD_{600} was measured for each culture to record bacterial biomass prior to centrifugation. Cultures were then centrifuged at 14,000 × *g* for 30 min at 4°C. Culture supernatants were collected and analyzed by LC–MS/MS to quantify leucine, isoleucine, and valine. All measured concentrations were normalized to the corresponding OD_{600} values to account for variations in bacterial cell density across groups.

Cell viability assay

Cell viability was assessed using the Cell Counting Kit-8 (CCK-8; Dojindo Laboratories, Kumamoto, Japan) assay in HepG2, HEK-293, and Caco-2 cells. Cells were seeded in 96-well plates at a density of 5,000 cells per well and allowed to attach for 24 h. Cells were then treated with Compound 1 or Compound 2 over a concentration range of 0.01–1,000 μM for 72 h. Control cells were treated with 0.1% DMSO vehicle. Subsequently, CCK-8 solution was added to each well at 10% of the culture volume, and plates were incubated for 1 h at 37°C. Absorbance was measured at 450 nm using a BioTek Epoch 2 microplate spectrophotometer (BioTek, Winooski, VT, USA). Cell viability was calculated as a percentage relative to the vehicle control group. Each treatment condition was tested in triplicate technical wells, and all experiments were independently repeated three times.

Langtaosha (LTS) Preprint doi: https://doi.org/10.65215/LTSpreprints.2026.11.27.000404. This version posted November 27, 2026. The copyright holder for this preprint (which was not certified by peer review) is the author/funder. Creative Commons license: CC Attribution-NonCommercial-NoDerivatives 4.0 https://creativecommons.org/licenses/by-nc-nd/4.0

Surface plasmon resonance analysis

All SPR reagents and consumables were from Cytiva. Binding kinetics between Compound 1 and *Bu*_DHAD or *Pv*_DHAD were measured using a Biacore 8K system (Cytiva) at 25 °C. Series S CM5 sensor chips were activated via amine coupling chemistry with a mixture of sulfo-N-hydroxysuccinimide and 1-ethyl-3-(3-dimethylaminopropyl) carbodiimide.

Compound 1 was serially diluted over a concentration range of 3.125–200 μM in PBS running buffer containing 0.5% DMSO; the DMSO concentration was kept consistent across all dilutions for solvent correction. Samples were injected at a flow rate of 30 μL/min, with association and dissociation phases of 100 s each.

Sensorgrams were analyzed using Biacore™ Insight Evaluation software (version 3.0). A 1:1 Langmuir binding model was fitted to the kinetic data to calculate the association rate constant (k_a), dissociation rate constant (k_d), and equilibrium dissociation constant (K_D).

***In vivo* validation of DHAD inhibitors**

Two cohorts of male C57BL/6J mice were used to evaluate the *in vivo* efficacy of DHAD inhibition. The first cohort consisted of 18-week-old mice maintained on an NCD (n = 16). The second cohort consisted of age-matched DIO mice (n = 16) that had been fed an HFD beginning at 6 weeks of age to establish diet-induced IR. Each cohort was randomly divided into two treatment groups (n = 8 per group).

Mice received daily oral gavage of Compound 1 at 25 mg/kg body weight or vehicle control consisting of 0.5% DMSO in PBS for 14 consecutive days. Dosing formulations were freshly prepared at a working concentration of 1 mg/mL. Administration volumes were adjusted according to individual body weight.

Fecal pellets were collected at baseline, after 7 days of treatment, and at the end of the 14-day treatment period for BCAA quantification by LC-MS/MS. OGTTs and ITTs were performed on days 7 and 14 according to the procedures described above. At the end of the treatment period, terminal blood samples were collected to quantify circulating BCAAs and serum markers of hepatic and renal function, including alanine aminotransferase, aspartate aminotransferase, and creatinine.

Colons were dissected, measured for total length, and fixed for hematoxylin and eosin staining. Stained sections were digitally imaged using an Olympus SLIDEVIEW VS200 slide scanner. Histological damage was graded on a 0–3 semi-quantitative scale in a blinded fashion, based on crypt architectural integrity and inflammatory cell infiltration: 0 = normal colonic structure with intact crypts and no inflammatory infiltration; 1 = mild damage with focal inflammatory infiltration and minimal crypt distortion; 2 = moderate damage with widespread inflammation and partial crypt loss; 3 = severe damage with extensive inflammation, complete crypt destruction and mucosal ulceration.

Langtaosha (LTS) Preprint doi: https://doi.org/10.65215/LTSpreprints.2026.11.27.000404. This version posted November 27, 2026. The copyright holder for this preprint (which was not certified by peer review) is the author/funder. Creative Commons license: CC Attribution-NonCommercial-NoDerivatives 4.0 https://creativecommons.org/licenses/by-nc-nd/4.0

For independent therapeutic validation, 7–8-week-old male *db/db* mice and age-matched wild-type *m/m* littermate controls (C57BLKS/J) were randomly assigned to receive Compound 1 or vehicle by daily oral gavage for 14 consecutive days (n = 8 per group). Dosing formulations and administration procedures were identical to those described above. Fecal samples were collected at baseline and on days 7 and 14 for longitudinal BCAA analysis. ITTs were performed, and fasting blood glucose (FBG) was measured after a 12-14 h fast, at the corresponding time points. Terminal serum samples were collected on day 14 for measurement of circulating BCAA concentrations.

Fecal microbiota composition analysis

Fecal samples were collected from NCD-fed and DIO mice, and total microbial genomic DNA was isolated from each sample. The bacterial 16S rRNA gene was amplified using 515F-806R, followed by paired-end sequencing on the Illumina NovaSeq 6000 platform (2 × 250 bp), with an average sequencing depth of ~60,000 reads per sample.

Raw sequencing data were processed using QIIME 2 (v2022.4.8). Sequence denoising and generation of the amplicon sequence variant table were performed using DADA2. Taxonomic classification was conducted against the SILVA 138.1 16S rRNA database.

All downstream diversity analyses were performed at the genus level. Alpha diversity was assessed using the Shannon and Chao1 indices. Beta diversity was evaluated using Bray–Curtis dissimilarity and visualized by principal coordinate analysis. Differences in overall community structure were assessed using permutational multivariate analysis of variance with 999 permutations.

Quantification of BCAA biosynthetic gene abundance

For the human gut metagenomic dataset shown in Figure 1B, BCAA biosynthetic genes were quantified using a targeted reference gene panel. Coding sequences corresponding to nine core BCAA biosynthetic genes—*ilvA*, *ilvBL*, *ilvBS*, *ilvC*, *ilvD*, *ilvE*, *leuA*, *leuB*, and *leuC*—from *B. uniformis* and *P. vulgatus* were compiled as reference sequences. Quality-filtered metagenomic reads were aligned to the reference gene panel. Mean gene abundance per sample was calculated using CoverM (v0.6.1) in “contig” mode, with the following parameters “--min-read-percent-identity 95 --min-read-aligned-percent 50”.

Independent human cohort for targeted validation

An independent clinical cohort comprising 100 participants, including 50 individuals with confirmed T2DM and 50 non-diabetic healthy controls, was used for targeted validation. Fecal samples from this cohort were analyzed for BCAA concentrations by targeted LC-

Langtaosha (LTS) Preprint doi: https://doi.org/10.65215/LTSpreprints.2026.11.27.000404. This version posted November 27, 2026. The copyright holder for this preprint (which was not certified by peer review) is the author/funder. Creative Commons license: CC Attribution-NonCommercial-NoDerivatives 4.0 https://creativecommons.org/licenses/by-nc-nd/4.0

MS/MS and for the abundances of *B. uniformis* and *P. vulgatus* by probe-based qPCR as mentioned above. Demographic and clinical characteristics are summarized in Table S7.

The study was approved by the Ethics Committee of Shenzhen University of Advanced Technology General Hospital, formerly Shenzhen Hospital of the University of Chinese Academy of Sciences (approval No. LL-KT-2020147). Written informed consent was obtained from all participants before sample collection.

Machine-learning-based prediction of IR-associated phenotypes

The discriminatory potential of the 52 bacterial species assigned to Cluster A was evaluated across multiple IR-associated metabolic disorders. The analysis included 1,251 metagenomic samples, comprising 495 samples from individuals with obesity, 226 from individuals with non-alcoholic fatty liver disease (NAFLD), 410 from individuals with atherosclerotic cardiovascular disease (ASCVD), and 120 from individuals with polycystic ovary syndrome (PCOS).

Raw sequencing data were quality-filtered using Sickle (v1.33).[48] Host-derived sequences were removed using BBMap (v35.x).[49] Species-level microbial abundance was quantified using CoverM (v0.6.1) with the parameters "--min-read-percent-identity 95 --min-read-aligned-percent 50" as stated previously.

The analytical workflow was implemented using the SIAMCAT R package. Microbial abundance profiles were subjected to feature filtering and log transformation before association analyses with the corresponding clinical phenotypes. A least absolute shrinkage and selection operator (LASSO)-regularized logistic regression model was constructed and evaluated using cross-validation.

Model performance was assessed using standard classification metrics, including ROC curves and AUC values. Feature-importance analyses were performed to identify microbial taxa contributing most strongly to disease classification. The predictive performance of the Cluster A signature was evaluated separately for each IR-associated metabolic disorder.

QUANTIFICATION AND STATISTICAL ANALYSIS

All statistical analyses were performed in R (v4.2.1). Microbial abundance and functional gene profiles were quantified using CoverM (v0.6.1), Salmon (v0.13.1), and the metaWRAP Quant_bins module with TPM normalization. BCAA concentrations were determined by targeted LC–MS/MS, and protein band intensities were quantified using ImageJ. Alpha diversity (Shannon and Chao1 indices) and beta diversity (Bray–Curtis PCoA) were calculated using QIIME 2 (v2022.4.8). Differential abundance analysis was performed using edgeR with false discovery rate (FDR) correction. Unless otherwise

Langtaosha (LTS) Preprint doi: https://doi.org/10.65215/LTSpreprints.2026.11.27.000404. This version posted November 27, 2026. The copyright holder for this preprint (which was not certified by peer review) is the author/funder. Creative Commons license: CC Attribution-NonCommercial-NoDerivatives 4.0 https://creativecommons.org/licenses/by-nc-nd/4.0

specified, pairwise between-group comparisons were performed using two-sided Welch's t-tests. Holm correction was applied for multiple related comparisons where indicated. Microbial taxonomic comparisons were performed using Wilcoxon rank-sum tests with Benjamini–Hochberg FDR correction where indicated. Time-course OGTT and ITT data were analyzed by two-way repeated-measures ANOVA followed by LSD post hoc tests. Differences in microbial community structure were assessed by PERMANOVA. Data are presented as mean ± SEM or mean ± SD, as indicated in the corresponding figure legends. A p-value < 0.05 was considered statistically significant (*p < 0.05; **p < 0.01; ***p < 0.001). Sample sizes are reported in the corresponding figure legends, and no data were excluded from analysis.

REFERENCES

1. Accili, D., Deng, Z., and Liu, Q. (2025). Insulin resistance in type 2 diabetes mellitus. Nat. Rev. Endocrinol. *21*, 413-426. https://doi.org/10.1038/s41574-025-01114-y.
2. Sun, H., Saeedi, P., Karuranga, S., Pinkepank, M., Ogurtsova, K., Duncan, B.B., Stein, C., Basit, A., Chan, J.C., and Mbanya, J.C. (2022). IDF Diabetes Atlas: Global, regional and country-level diabetes prevalence estimates for 2021 and projections for 2045. Diabetes Res. Clin. Pract. *183*, 109119. https://doi.org/10.1016/j.diabres.2021.109119.
3. Shurrab, N.T., and Arafa, E.-S.A. (2020). Metformin: A review of its therapeutic efficacy and adverse effects. Obes. Med. *17*, 100186. https://doi.org/10.1016/j.obmed.2020.100186.
4. Zhu, T., and Goodarzi, M.O. (2020). Metabolites linking the gut microbiome with risk for type 2 diabetes. Curr. Nutr. Rep. *9*, 83-93. https://doi.org/10.1007/s13668-020-00307-3.
5. Donia, M.S., and Fischbach, M.A. (2015). Small molecules from the human microbiota. Science *349*, 1254766. https://doi.org/10.1126/science.1254766.
6. Koh, A., Molinaro, A., Ståhlman, M., Khan, M.T., Schmidt, C., Mannerås-Holm, L., Wu, H., Carreras, A., Jeong, H., and Olofsson, L.E. (2018). Microbially produced imidazole propionate impairs insulin signaling through mTORC1. Cell *175*, 947-961. https://doi.org/10.1016/j.cell.2018.09.055.
7. Yang, Q., Vijayakumar, A., and Kahn, B.B. (2018). Metabolites as regulators of insulin sensitivity and metabolism. Nat. Rev. Mol. Cell Biol. *19*, 654-672. https://doi.org/10.1038/s41580-018-0044-8.
8. Baars, D.P., Fondevila, M.F., Meijnikman, A.S., and Nieuwdorp, M. (2024). The central role of the gut microbiota in the pathophysiology and management of type 2 diabetes. Cell Host Microbe *32*, 1280-1300. https://doi.org/10.1016/j.chom.2024.07.017.
9. Nicklin, P., Bergman, P., Zhang, B., Triantafellow, E., Wang, H., Nyfeler, B., Yang, H., Hild, M., Kung, C., and Wilson, C. (2009). Bidirectional transport of amino acids regulates mTOR and autophagy. Cell *136*, 521-534.

Langtaosha (LTS) Preprint doi: https://doi.org/10.65215/LTSpreprints.2026.11.27.000404. This version posted November 27, 2026. The copyright holder for this preprint (which was not certified by peer review) is the author/funder. Creative Commons license: CC Attribution-NonCommercial-NoDerivatives 4.0 https://creativecommons.org/licenses/by-nc-nd/4.0

https://doi.org/10.1016/j.cell.2008.11.044.

10. Newgard, C.B., An, J., Bain, J.R., Muehlbauer, M.J., Stevens, R.D., Lien, L.F., Haqq, A.M., Shah, S.H., Arlotto, M., and Slentz, C.A. (2009). A branched-chain amino acid-related metabolic signature that differentiates obese and lean humans and contributes to insulin resistance. Cell Metab. *9*, 311-326. https://doi.org/10.1016/j.cmet.2009.02.002.
11. Choi, B.H., Hyun, S., and Koo, S.-H. (2024). The role of BCAA metabolism in metabolic health and disease. Exp. Mol. Med. *56*, 1552-1559. https://doi.org/10.1038/s12276-024-01263-6.
12. Karusheva, Y., Koessler, T., Strassburger, K., Markgraf, D., Mastrototaro, L., Jelenik, T., Simon, M.-C., Pesta, D., Zaharia, O.-P., and Bódis, K. (2019). Short-term dietary reduction of branched-chain amino acids reduces meal-induced insulin secretion and modifies microbiome composition in type 2 diabetes: a randomized controlled crossover trial. Am. J. Clin. Nutr. *110*, 1098-1107. https://doi.org/10.1093/ajcn/nqz191.
13. Layman, D.K. (2003). The role of leucine in weight loss diets and glucose homeostasis. J. Nutr. *133*, 261S-267S. https://doi.org/10.1093/jn/133.1.261S.
14. Biswas, D., Duffley, L., and Pulinilkunnil, T. (2019). Role of branched-chain amino acid–catabolizing enzymes in intertissue signaling, metabolic remodeling, and energy homeostasis. FASEB J. *33*, 8711-8731. https://doi.org/10.1096/fj.201802842RR.
15. Pedersen, H.K., Gudmundsdottir, V., Nielsen, H.B., Hyotylainen, T., Nielsen, T., Jensen, B.A., Forslund, K., Hildebrand, F., Prifti, E., and Falony, G. (2016). Human gut microbes impact host serum metabolome and insulin sensitivity. Nature *535*, 376-381. https://doi.org/10.1038/nature18646.
16. Hoyles, L., Fernández-Real, J.-M., Federici, M., Serino, M., Abbott, J., Charpentier, J., Heymes, C., Luque, J.L., Anthony, E., and Barton, R.H. (2018). Molecular phenomics and metagenomics of hepatic steatosis in non-diabetic obese women. Nat. Med. *24*, 1070-1080. https://doi.org/10.1038/s41591-018-0061-3.
17. Kim, J., and Guan, K.-L. (2019). mTOR as a central hub of nutrient signalling and cell growth. Nat. Cell Biol. *21*, 63-71. https://doi.org/10.1038/s41556-018-0205-1.
18. Raj, T., Dileep, U., Vaz, M., Fuller, M.F., and Kurpad, A.V. (2008). Intestinal microbial contribution to metabolic leucine input in adult men. J. Nutr. *138*, 2217-2221. https://doi.org/10.3945/jn.108.093021.
19. Roth Flach, R.J., Bollinger, E., Reyes, A.R., Laforest, B., Kormos, B.L., Liu, S., Reese, M.R., Martinez Alsina, L.A., Buzon, L., and Zhang, Y. (2023). Small molecule branched-chain ketoacid dehydrogenase kinase (BDK) inhibitors with opposing effects on BDK protein levels. Nat. Commun. *14*, 4812. https://doi.org/10.1038/s41467-023-40536-y.
20. Tambets, R., Jesse, M., Kronberg, J., van der Graaf, A., Abner, E., Võsa, U., Rahu, I., Taba, N., Kolde, A., and Yarish, D. (2026). Genetic analysis of circulating metabolic traits in 619,372 individuals. Nature *655*, 971-978.

Langtaosha (LTS) Preprint doi: https://doi.org/10.65215/LTSpreprints.2026.11.27.000404. This version posted November 27, 2026. The copyright holder for this preprint (which was not certified by peer review) is the author/funder. Creative Commons license: CC Attribution-NonCommercial-NoDerivatives 4.0 https://creativecommons.org/licenses/by-nc-nd/4.0

https://doi.org/10.1038/s41586-026-10532-5.

21. Sun, Y., Nie, Q., Zhang, S., He, H., Zuo, S., Chen, C., Yang, J., Chen, H., Hu, J., Li, S., et al. (2023). *Parabacteroides distasonis* ameliorates insulin resistance via activation of intestinal GPR109a. Nat. Commun. *14*, 7740. https://doi.org/10.1038/s41467-023-43622-3.
22. Lin, J., Nie, Q., Cheng, J., Zhong, Y.-N., Zhang, T., Zhang, X., Ge, X., Ding, Y., Niu, C., and Gao, Y. (2025). A microbial amino-acid-conjugated bile acid, tryptophan-cholic acid, improves glucose homeostasis via the orphan receptor MRGPRE. Cell *188*, 4530-4548. https://doi.org/10.1016/j.cell.2025.05.010.
23. Wallace, B.D., Wang, H., Lane, K.T., Scott, J.E., Orans, J., Koo, J.S., Venkatesh, M., Jobin, C., Yeh, L.-A., and Mani, S. (2010). Alleviating cancer drug toxicity by inhibiting a bacterial enzyme. Science *330*, 831-835. https://doi.org/10.1126/science.1191175.
24. Maini Rekdal, V., Bess, E.N., Bisanz, J.E., Turnbaugh, P.J., and Balskus, E.P. (2019). Discovery and inhibition of an interspecies gut bacterial pathway for Levodopa metabolism. Science *364*, eaau6323. https://doi.org/10.1126/science.aau6323.
25. Creasy, H.H., Felix, V., Aluvathingal, J., Crabtree, J., Ifeonu, O., Matsumura, J., McCracken, C., Nickel, L., Orvis, J., and Schor, M. (2021). HMPDACC: a human microbiome project multi-omic data resource. Nucleic Acids Res. *49*, D734-D742. https://doi.org/10.1093/nar/gkaa996.
26. Jie, Z., Xia, H., Zhong, S.-L., Feng, Q., Li, S., Liang, S., Zhong, H., Liu, Z., Gao, Y., and Zhao, H. (2017). The gut microbiome in atherosclerotic cardiovascular disease. Nat. Commun. *8*, 845. https://doi.org/10.1038/s41467-017-00900-1.
27. Karlsson, F.H., Tremaroli, V., Nookaew, I., Bergström, G., Behre, C.J., Fagerberg, B., Nielsen, J., and Bäckhed, F. (2013). Gut metagenome in European women with normal, impaired and diabetic glucose control. Nature *498*, 99-103. https://doi.org/10.1038/nature12198.
28. Qin, J., Li, R., Raes, J., Arumugam, M., Burgdorf, K.S., Manichanh, C., Nielsen, T., Pons, N., Levenez, F., and Yamada, T. (2010). A human gut microbial gene catalogue established by metagenomic sequencing. Nature *464*, 59-65. https://doi.org/10.1038/nature08821.
29. Qin, J., Li, Y., Cai, Z., Li, S., Zhu, J., Zhang, F., Liang, S., Zhang, W., Guan, Y., and Shen, D. (2012). A metagenome-wide association study of gut microbiota in type 2 diabetes. Nature *490*, 55-60. https://doi.org/10.1038/nature11450.
30. Yan, Y., Liu, Q., Zang, X., Yuan, S., Bat-Erdene, U., Nguyen, C., Gan, J., Zhou, J., Jacobsen, S.E., and Tang, Y. (2018). Resistance-gene-directed discovery of a natural-product herbicide with a new mode of action. Nature *559*, 415-418. https://doi.org/10.1038/s41586-018-0319-4.
31. He, B., Hu, Y., Liu, D., Zang, X., He, X., Chen, W., Yang, J., Feng, M., Chen, P., and Wei, L. (2025). Substrate-based discovery of α-hydroxycarboxylic acid derivatives as potential herbicides targeting dihydroxyacid dehydratase. Nat. Commun. *16*, 5205. https://doi.org/10.1038/s41467-025-60489-8.
32. He, B., Hu, Y., He, X., Chen, W., Yan, W., Zang, X., Zhou, J., and Ye, Y. (2025).

Langtaosha (LTS) Preprint doi: https://doi.org/10.65215/LTSpreprints.2026.11.27.000404. This version posted November 27, 2026. The copyright holder for this preprint (which was not certified by peer review) is the author/funder. Creative Commons license: CC Attribution-NonCommercial-NoDerivatives 4.0 https://creativecommons.org/licenses/by-nc-nd/4.0

De novo design and synthesis of novel benzoxazinone derivatives targeting dihydroxyacid dehydratase. Plant Biotechnol. J. https://doi.org/10.1111/pbi.70369.

33. Zhai, L., Xiao, H., Lin, C., Wong, H.L.X., Lam, Y.Y., Gong, M., Wu, G., Ning, Z., Huang, C., and Zhang, Y. (2023). Gut microbiota-derived tryptamine and phenethylamine impair insulin sensitivity in metabolic syndrome and irritable bowel syndrome. Nat. Commun. *14*, 4986. https://doi.org/10.1038/s41467-023-40552-y.

34. Jang, C., Oh, S.F., Wada, S., Rowe, G.C., Liu, L., Chan, M.C., Rhee, J., Hoshino, A., Kim, B., and Ibrahim, A. (2016). A branched-chain amino acid metabolite drives vascular fatty acid transport and causes insulin resistance. Nat. Med. *22*, 421-426. https://doi.org/10.1038/nm.4057.

35. Felig, P., Marliss, E., and Cahill Jr, G.F. (1969). Plasma amino acid levels and insulin secretion in obesity. New Engl. J. Med. *281*, 811-816. https://doi.org/10.1056/NEJM196910092811503.

36. Bayaraa, T., Gaete, J., Sutiono, S., Kurz, J., Lonhienne, T., Harmer, J.R., Bernhardt, P.V., Sieber, V., Guddat, L., and Schenk, G. (2022). Dihydroxy-acid dehydratases from pathogenic bacteria: emerging drug targets to combat antibiotic resistance. Chem. Eur. J. *28*, e202200927. https://doi.org/10.1002/chem.202200927.

37. Tong, J., Liu, C., Summanen, P., Xu, H., and Finegold, S.M. (2011). Application of quantitative real-time PCR for rapid identification of *Bacteroides fragilis* group and related organisms in human wound samples. Anaerobe *17*, 64-68.

38. Zheng, L., Tan, Y., Hu, Y., Shen, J., Qu, Z., Chen, X., Ho, C.L., Leung, E.L.-H., Zhao, W., and Dai, L. (2022). CRISPR/Cas-based genome editing for human gut commensal *Bacteroides* species. ACS Synth. Biol. *11*, 464-472. https://doi.org/10.1021/acssynbio.1c00543.

39. Uritskiy, G.V., DiRuggiero, J., and Taylor, J. (2018). MetaWRAP—a flexible pipeline for genome-resolved metagenomic data analysis. Microbiome *6*, 158. https://doi.org/10.1186/s40168-018-0541-1.

40. Chaumeil, P.-A., Mussig, A.J., Hugenholtz, P., and Parks, D.H. (2022). GTDB-Tk v2: memory friendly classification with the genome taxonomy database. Bioinformatics *38*, 5315-5316. https://doi.org/10.1093/bioinformatics/btac672.

41. Olm, M.R., Brown, C.T., Brooks, B., and Banfield, J.F. (2017). dRep: a tool for fast and accurate genomic comparisons that enables improved genome recovery from metagenomes through de-replication. ISME J. *11*, 2864-2868. https://doi.org/10.1038/ismej.2017.126.

42. Parks, D.H., Imelfort, M., Skennerton, C.T., Hugenholtz, P., and Tyson, G.W. (2015). CheckM: assessing the quality of microbial genomes recovered from isolates, single cells, and metagenomes. Genome Res. *25*, 1043-1055. https://doi.org/10.1101/gr.186072.114.

43. Minh, B.Q., Schmidt, H.A., Chernomor, O., Schrempf, D., Woodhams, M.D., Von Haeseler, A., and Lanfear, R. (2020). IQ-TREE 2: new models and efficient methods for phylogenetic inference in the genomic era. Mol. Biol. Evol. *37*,

Langtaosha (LTS) Preprint doi: https://doi.org/10.65215/LTSpreprints.2026.11.27.000404. This version posted November 27, 2026. The copyright holder for this preprint (which was not certified by peer review) is the author/funder. Creative Commons license: CC Attribution-NonCommercial-NoDerivatives 4.0 https://creativecommons.org/licenses/by-nc-nd/4.0

1530-1534. https://doi.org/10.1093/molbev/msaa015.

44. Letunic, I., and Bork, P. (2024). Interactive Tree of Life (iTOL) v6: recent updates to the phylogenetic tree display and annotation tool. Nucleic Acids Res. *52*, W78-W82. https://doi.org/10.1093/nar/gkae268.

45. Patro, R., Duggal, G., Love, M.I., Irizarry, R.A., and Kingsford, C. (2017). Salmon provides fast and bias-aware quantification of transcript expression. Nat. Methods *14*, 417-419. https://doi.org/10.1038/nmeth.4197.

46. Pritchard, L., Cock, P., and Esen, Ö. (2019). pyani v0.2.8: average nucleotide identity (ANI) and related measures for whole genome comparisons. https://doi.org/10.5281/zenodo.2584238.

47. Huerta-Cepas, J., Forslund, K., Coelho, L.P., Szklarczyk, D., Jensen, L.J., von Mering, C., and Bork, P. (2017). Fast genome-wide functional annotation through orthology assignment by eggNOG-mapper. Mol. Biol. Evol. *34*, 2115-2122. https://doi.org/10.1093/molbev/msx148.

48. Joshi, N., and Fass, J. (2011). Sickle: A sliding-window, adaptive, quality-based trimming tool for FastQ files (Version 1.33)[Software].

49. Bushnell, B. (2014). BBMap: a fast, accurate, splice-aware aligner. 9th Annual Genomics of Energy & Environment Meeting.

50. Bowers, R.M., Kyrpides, N.C., Stepanauskas, R., Harmon-Smith, M., Doud, D., Reddy, T.B.K., Schulz, F., Jarett, J., Rivers, A.R., Eloe-Fadrosh, E.A., et al. (2017). Minimum information about a single amplified genome (MISAG) and a metagenome-assembled genome (MIMAG) of bacteria and archaea. Nat. Biotechnol. *35*, 725-731. https://doi.org/10.1038/nbt.3893.

51. Konstantinidis, K.T., Rosselló-Móra, R., and Amann, R. (2017). Uncultivated microbes in need of their own taxonomy. ISME J. *11*, 2399. https://doi.org/10.1038/ismej.2017.113.

52. Nearing, J.T., Douglas, G.M., Hayes, M.G., MacDonald, J., Desai, D.K., Allward, N., Jones, C.M., Wright, R.J., Dhanani, A.S., and Comeau, A.M. (2022). Microbiome differential abundance methods produce different results across 38 datasets. Nat. Commun. *13*, 342. https://doi.org/10.1038/s41467-022-28034-z.

53. Chen, Y., Chen, L., Lun, A.T., Baldoni, P.L., and Smyth, G.K. (2025). edgeR v4: powerful differential analysis of sequencing data with expanded functionality and improved support for small counts and larger datasets. Nucleic Acids Res. *53*, gkaf018. https://doi.org/10.1093/nar/gkaf018.

54. Lim, B., Zimmermann, M., Barry, N.A., and Goodman, A.L. (2017). Engineered regulatory systems modulate gene expression of human commensals in the gut. Cell *169*, 547-558. e515. https://doi.org/10.1016/j.cell.2017.03.045.

55. Suárez-Zamorano, N., Fabbiano, S., Chevalier, C., Stojanović, O., Colin, D.J., Stevanović, A., Veyrat-Durebex, C., Tarallo, V., Rigo, D., and Germain, S. (2015). Microbiota depletion promotes browning of white adipose tissue and reduces obesity. Nat. Med. *21*, 1497-1501. https://doi.org/10.1038/nm.3994.

56. Almeida, A., Nayfach, S., Boland, M., Strozzi, F., Beracochea, M., Shi, Z.J., Pollard, K.S., Sakharova, E., Parks, D.H., and Hugenholtz, P. (2021). A unified catalog of 204,938 reference genomes from the human gut microbiome. Nat.

Langtaosha (LTS) Preprint doi: https://doi.org/10.65215/LTSpreprints.2026.11.27.000404. This version posted November 27, 2026. The copyright holder for this preprint (which was not certified by peer review) is the author/funder. Creative Commons license: CC Attribution-NonCommercial-NoDerivatives 4.0 https://creativecommons.org/licenses/by-nc-nd/4.0

Biotechnol. *39*, 105-114. https://doi.org/10.1038/s41587-020-0603-3.

57. Kanehisa, M., and Goto, S. (2000). KEGG: kyoto encyclopedia of genes and genomes. Nucleic Acids Res. *28*, 27-30. https://doi.org/10.1093/nar/28.1.27.

58. Alcock, J., and Lin, H.C. (2015). Fatty acids from diet and microbiota regulate energy metabolism. F1000Research *4*. https://doi.org/10.12688/f1000research.6078.1.

59. Brown, E.M., Clardy, J., and Xavier, R.J. (2023). Gut microbiome lipid metabolism and its impact on host physiology. Cell Host Microbe *31*, 173-186. https://doi.org/10.1016/j.chom.2023.01.009.

60. Canfora, E.E., Meex, R.C., Venema, K., and Blaak, E.E. (2019). Gut microbial metabolites in obesity, NAFLD and T2DM. Nat. Rev. Endocrinol. *15*, 261-273. https://doi.org/10.1038/s41574-019-0156-z.

61. Carbonero, F., Benefiel, A.C., Alizadeh-Ghamsari, A.H., and Gaskins, H.R. (2012). Microbial pathways in colonic sulfur metabolism and links with health and disease. Front. Physiol. *3*, 448. https://doi.org/10.3389/fphys.2012.00448.

62. Jameson, E., Quareshy, M., and Chen, Y. (2018). Methodological considerations for the identification of choline and carnitine-degrading bacteria in the gut. Methods *149*, 42-48. https://doi.org/10.1016/j.ymeth.2018.03.012.

63. Krautkramer, K.A., Fan, J., and Bäckhed, F. (2021). Gut microbial metabolites as multi-kingdom intermediates. Nat. Rev. Microbiol. *19*, 77-94. https://doi.org/10.1038/s41579-020-0438-4.

64. Pedret, A., Valls, R.M., Calderón-Pérez, L., Llauradó, E., Companys, J., Pla-Pagà, L., Moragas, A., Martín-Luján, F., Ortega, Y., and Giralt, M. (2019). Effects of daily consumption of the probiotic *Bifidobacterium animalis* subsp. lactis CECT 8145 on anthropometric adiposity biomarkers in abdominally obese subjects: a randomized controlled trial. Int. J. Obes. *43*, 1863-1868. https://doi.org/10.1038/s41366-018-0220-0.

65. Pickersgill, L., Litherland, G.J., Greenberg, A.S., Walker, M., and Yeaman, S.J. (2007). Key role for ceramides in mediating insulin resistance in human muscle cells. J. Biol. Chem. *282*, 12583-12589. https://doi.org/10.1074/jbc.M611157200.

66. Roager, H., and Dragsted, L. (2019). Diet-derived microbial metabolites in health and disease. Nutr. Bull. *44*, 216-227. https://doi.org/10.1111/nbu.12396.

67. Simó, C., and García-Cañas, V. (2020). Dietary bioactive ingredients to modulate the gut microbiota-derived metabolite TMAO. New opportunities for functional food development. Food Funct. *11*, 6745-6776. https://doi.org/10.1039/d0fo01237h.

68. Singh, S.B., and Lin, H.C. (2015). Hydrogen sulfide in physiology and diseases of the digestive tract. Microorganisms *3*, 866-889. https://doi.org/10.3390/microorganisms3040866.

69. Xu, F., Tavintharan, S., Sum, C.F., Woon, K., Lim, S.C., and Ong, C.N. (2013). Metabolic signature shift in type 2 diabetes mellitus revealed by mass spectrometry-based metabolomics. J. Clin. Endocrinol. Metab. *98*, E1060-E1065. https://doi.org/10.1210/jc.2012-4132.

Langtaosha (LTS) Preprint doi: https://doi.org/10.65215/LTSpreprints.2026.11.27.000404. This version posted November 27, 2026. The copyright holder for this preprint (which was not certified by peer review) is the author/funder. Creative Commons license: CC Attribution-NonCommercial-NoDerivatives 4.0 https://creativecommons.org/licenses/by-nc-nd/4.0